# Comparative degradation behavior of carbonate apatite-coated and hydroxyapatite-coated Mg-Ca alloy plates and screws in rabbit femurs

Sachiko Hiromoto [a*], Etsuro Nozoe [b], Kotaro Hanada [c], Takuya Yoshimura [b], Kaori Shima [b], Norifumi Nakamura [b], and Aya Chiba [a]

[a] *Research Center for Structural Materials, National Institute for Materials Science (NIMS), Tsukuba, Japan,* [b] *Graduate School of Medical and Dental Sciences, Kagoshima University, Kagoshima, Japan,* [c] *Advanced Manufacturing Research Institute, National Institute of Advanced Industrial Science and Technology (AIST), Tsukuba, Japan*

* Corresponding author: S. Hiromoto

Corrosion and Protection Group, Research Center for Structural Materials, National Institute for Materials Science; 1-2-1 Sengen, Tsukuba 305-0047, Japan; Tel. +81-29-859-2610; E-mail address hiromoto.sachiko@nims.go.jp

**Abstract**

Carbonate apatite (CAp) and hydroxyapatite (HAp) coatings were formed on Mg-0.8mass% Ca (MgCa) alloy plates and screws as bioabsorbable and non-absorbable corrosion suppression coatings, respectively, and implanted in rabbit femurs alongside uncoated devices for 8 and 24 weeks. The degradation behavior of CAp-coated and HAp-coated MgCa, as well as the surrounding bone formation were investigated using scanning electron microscopy and histological observations. The CAp and HAp coatings effectively suppressed the initial rapid corrosion of MgCa devices. Subsequently, while the CAp-coated devices showed no apparent corrosion pits, the HAp-coated devices showed millimeter-sized pits. The 24-week mean corrosion rate of CAp-coated devices was about half that of HAp-coated devices and about one-fifth of uncoated devices. Initially, both CAp and HAp coatings equivalently enhanced new bone formation, promoting screw-bone bonding. However, over time, the screw-bone bonding remained unchanged for CAp-coated screws, whereas it decreased for HAp-coated screws due to substrate corrosion and dissolution of corrosion products. Notably, the CAp coating began to dissolve between 8 and 24 weeks without harming the surrounding tissue, particularly in areas where new bone had adhered. In contrast, the HAp coating almost remained its original shape. It was demonstrated that the CAp coating can effectively suppress MgCa device corrosion and gradually dissolve over time.

Keywords: word; carbonate apatite coating; biomedical magnesium alloys; rabbit femur: in vivo degradation: bioabsorbable coating; biomaterial

## 1. Introduction

Magnesium (Mg) and Mg alloys have been examined as next-generation biodegradable materials with good biocompatibility and mechanical compatibility for bone fixation plates and screws, pins, mesh plates and so on. Compared to biodegradable polymers, Mg/Mg alloys show higher strength, while their Young's modulus (40-45 GPa) is lower than that of conventional metallic materials such as titanium alloys and stainless steels [1-6]. However, clinical trials have revealed that Mg/Mg alloys sometimes show too rapid corrosion in the early stages after implantation, leading to early degradation of mechanical integrity, gas cavity formation due to hydrogen ($H_2$) gas, and pH increase caused by $OH^-$ ions [7-14]. Although the gas cavities eventually disappear as they are filled with the surrounding tissues [15], concerns remain that they may interfere with tissue regeneration.

To overcome the issue of the initial rapid corrosion of Mg/Mg alloys, various surface modifications such as calcium phosphate compounds, $MgF_2$, $Mg(OH)_2$, and micro-arc oxidation (MAO) coatings have been developed [4, 5, 16-28]. Among these, calcium phosphate coatings, such as hydroxyapatite (HAp), β-tricalcium phosphate (β-TCP), octacalcium phosphate (OCP) and dicalcium phosphate dihydrate (DCPD), have been extensively developed because these coatings promote bonding to surrounding bone due to their excellent bone compatibility. For example, a β-TCP coating reduced the corrosion amount of Mg-3mass% Al-1mass% Zn (AZ31) by about half at 12 weeks post-implantation in rat femurs and promoted new bone formation by releasing $Ca^{2+}$ and $PO_4^{3-}$ ions from the coating [17]. Similarly, a HAp coating mitigated the degradation of pure Mg for the first 6 weeks in rabbit tibial shafts and significantly enhanced bone growth [18]. Cheng et al. reported that HAp-coated pure Mg, despite showing the best

in vivo corrosion resistance in rat femurs for 8 weeks, showed rather less bone formation that $MgF_2$-coated pure Mg [24].

Our research focuses on developing HAp and carbonate apatite (CAp) coatings as non-absorbable and bioabsorbable coatings, respectively, using various Mg/Mg alloys such as pure Mg, AZ31, Mg-4mass% Y-3mass% rare earth (WE43) [29-33]. HAp was first employed because apatite is the main component of bone and shows high bone conduction property [32] and because HAp is practically used as an artificial bone substitute and a coating material for Ti alloy implants to promote bone formation [34-36]. Therefore, the HAp coating is expected not only to suppress the corrosion rate of Mg alloys, but also to promote bonding with the surrounding bone. It was found that the developed HAp coatings effectively prevent gas cavity formation in mouse subcutaneous tissue and in rat femurs by suppressing Mg/Mg alloy corrosion [31, 37], while promoting bone formation [37]. It was also found that the HAp coatings remained almost unchanged even after 24 weeks and were fragmented into pieces as substrate Mg/Mg alloys thinned due to corrosion [37]. These results showed the need for bioabsorbable coatings. Therefore, we focused on CAp coatings due to the following characteristics of CAp. The composition of CAp ($Ca_{10-a}(PO_4)_{6-b}(CO_2)_c(OH)_{2-d}$) is closer to that of bone apatite than HAp. CAp is characterized by an increase in solubility with decreasing pH, although its solubility is low at around the in vivo pH 7.5, and is normally stable, but is dissolved by HCl secreted by osteoclasts. CAp is thus used as absorbable artificial bone substitute [38, 39]. In the case of β-TCP, which is also used as an absorbable artificial bone substitute, its high solubility around pH 7.5 suggests that it begins dissolving immediately after in vivo implantation. Based on these dissolution characteristics, CAp coatings are expected to remain stable to maintain the mechanical integrity of the substrate Mg alloys until the surrounding bone heals, after which it will

dissolve and be absorbed by osteoclasts, when they are used for orthopedic and dental devices. Additionally, the solubility of CAp can be controlled by its carbonate content [38], and thus the corrosion of CAp-coated Mg/Mg alloy is expected to vary with the carbonate content.

We previously developed CAp coatings with different carbonate contents [32, 33]. It was revealed in cell culture tests that the CAp coatings were absorbed by osteoclasts, whereas a HAp coating was not [32]. Interestingly, the CAp coatings showed equivalent corrosion suppression ability to the HAp coating for WE43 in a culture medium with and without osteoclasts although the CAp coatings were partly degraded with osteoclasts [32, 40]. However, it remains unknown whether the CAp coatings can exhibit equivalent in vivo corrosion suppression ability to the HAp coatings and whether they can be absorbed in vivo. This is because it has been well known that in vivo corrosion rates of Mg alloys are often different from in vitro corrosion rates [41] and because the chemical and physicochemical environments, such as pH and diffusivity, are different between culture environments and in vivo environments.

In this study, the CAp and HAp coatings were formed on Mg-0.8mass% Ca (MgCa) devices of plate and screw and implanted in rabbit femurs with uncoated devices to compare the influence of CAp and HAp coatings on the corrosion behavior of substrate MgCa alloy and the difference in the degradation behavior of the coatings. Moreover, histological studies of bone formed around the implanted devices was examined with hematoxylin-eosin (HE) and toluidine blue (TB) staining. The implantation period was 8 weeks, when the bone was expected to have healed, and 24 weeks, when the MgCa alloy was expected to have mostly corroded.

## 2. Experimental

### *2.1. CAp and HAp coating procedure*

Mg-0.8mass% Ca (MgCa) alloy plate and screw with a size shown in Fig. 1 were used as a substrate. The composition of the MgCa alloy used are shown in Table 1. The MgCa alloy exhibits a proof stress of 144±4.9 MPa, a tensile strength of 224±0.9 MPa and an elongation to failure of 21.0±2.5%. Plates and screws were fabricated by dry machining from MgCa extrusion rod, degreased with acetone, and used as uncoated samples.

CAp and HAp coatings were formed on the MgCa plates and screws by previously reported method [32]. Coating solutions of 0.2 mol/L ethylenediaminetetraacetic acid calcium disodium salt hydrate ($C_{10}H_{12}CaN_2Na_2O_8 \cdot xH_2O$), 0.2 mol/L potassium dihydrogen phosphate ($KH_2PO_4$) and 0 or 0.5 mol/L sodium hydrogen carbonate ($NaHCO_3$) were prepared with the pH adjusted to 8-9 with 1 mol/L sodium hydroxide (NaOH) solution [32]. The chemicals used for coating were reagent grade. The coating solutions were heated to 363 K and then MgCa plates and screws were immersed for 1 h. Formation of CAp and HAp coatings were examined by X-ray diffraction measurement (XRD, D2 Phaser, Bruker) using Cu Kα radiation and diffuse reflectance FTIR (IRTracer-100, Shimadzu) measurement at 4 $cm^{-1}$ resolution. For XRD measurements, several plates or screws were closely aligned on the sample table to obtain sufficient signal. Morphology and composition of the coatings were analyzed using scanning electron microscope (SEM: FEI, Quanta FEG 250) equipped with energy dispersion X-ray spectroscopy (EDS: TEAM EDS, EDAX). To prevent contamination of the sample surface, the samples were only placed on the sample stage, limiting the resolution of SEM images and the accuracy of EDS analysis. The relative atomic ratios of Ca to P and total Ca, Na and K to P (Ca/P ratio and (Ca+Na+K)/P ratio) were obtained. Due to the limited number of samples, the cross section was observed only for the CAp-coated

screw that was screwed into a femur once and immediately removed because the screw head was accidentally broken, using SEM (Miniscope TM3030, Hitachi). The cross section of the other as-prepared coatings could not be observed.

### *2.2. Implantation test in rabbit femurs*

Japanese white rabbits (KBT-JW) of female with 3.0-3.5 kg weight were used. The animal experiments were approved with the approval number D20008 by the Institutional Animal Experiment Committee of Kagoshima University in Japan. Screw holes were drilled in femurs with an electric drill using a stainless-steel round bar with a diameter of 0.8 mm, and then the holes were widened with drills with a diameter of 1.2 mm and 1.5 mm. Subsequently, a set of one plate and three screws was fixed to each femur as shown in Fig. 2. The uncoated and CAp/HAp-coated device sets were implanted into one and the other femur of the same rabbit, respectively. Three sets of devices with each surface were implanted. The implantation procedure was performed by the same surgeon to avoid any change in the technique. The implantation period was 8 and 24 weeks.

X-ray photographs were taken under sedation using dental radiography equipment (portable X-ray IME-100A, TOSHIBA MEDICAL and FCR Pico system V, Fujifilm) at 1, 4 , 8 , 12, 18 and 24 weeks. At 8 or 24 weeks, euthanasia was performed by intravenous injection of pentobarbital (80-100 mg/kg). The femurs with devices were harvested, dehydrated and fixed with a 10% buffered formalin, and then embedded in epoxy resin. The plates with femurs in resin were cut between hip side screw and center screw as illustrated in Fig. 2, and then X-ray 3D μCT images of the femurs with devices were taken using a microcomputed tomography (SKYSCAN 1174, Bruker) with

resolution of 6.6 μm/pixel. The total bone length in contact with each screw was measured using μCT images as show in Fig. 2.

Then, the samples with two screws were cut in half along the longitudinal direction of femurs as illustrated in Fig. 2, and the cross sections were mirror-finished. Low and high magnification SEM observations of the cross sections were carried out using SEM (Miniscope TM3030 or Quanta FEG 250) with EDS after depositing carbon on the cross sections. The resolution of the SEM images was limited because the samples were embedded in a resin block, which prevented the plates and screws from conducting with the sample stage.

Cross-sectional area of remaining metal parts of each screw and that of plate sandwiched between screws were obtained from the cross-sectional images using ImageJ (NIH). Here, the cross-sectional area of screws that were cut at an angle and were extremely short in length was not included in the mean cross-sectional area. The ratio of remaining area to original area was calculated, using the original area of plate and screw as about 9 $mm^2$ and 12 $mm^2$, respectively. Additionally, the mean corrosion thinning rate for 0-8 and 0-24 weeks was calculated, assuming that the screw was a 7 mm long and 2 mm diameter rod and the measurement part of the plate was a 7.5 mm long and 1 mm thickness plate. It was also assumed that the plates and screws corroded uniformly.

Differences between specimens in the bone contact length and in the ratio of remaining metal area to original area were compared using a repeated measure analysis of variance (ANOVA) using Statcel4 on Excel for Office 365. When significant difference was indicated, Tukey–Kramer test was carried out as a post-hoc test.

The samples with two screws were stained with toluidine blue (TB)(CHROMA), and those with one screw were stained with hematoxylin-eosin (HE) for the histological

observation of bone formed around the screws and for examining inflammatory cell infiltration. Then, the stained samples were observed using optical microscope (BZ-X710, KEYENCE).

## 3. Results

### *3.1. CAp and HAp coating of MgCa plates and screws*

Figure 3(a)-(d) shows the optical images of the as-prepared CAp-coated and HAp-coated plates and screws and Fig. 3(e)-(h) shows the low and high magnification surface SEM images. Figure 3(i) shows the cross-sectional SEM image of the CAp coated screw. Regardless of the uneven shape of devices, the CAp and HAp coatings uniformly covered the surface, as all plates and screws are uniformly colored as shown in Fig. 3(a)-(d). The CAp coating consisted of a dense agglomerate of sub-micrometer to 1 μm particles (Fig. 3(e) and (f)), and the thickness was about 1 μm (Fig. 3(i)), which is comparable to the CAp coating of WE43 and pure Mg disks formed under the same condition [32, 33]. The HAp coating consisted of a dense agglomerate of 1-3 μm particles (Fig. 3(g) and (h)). As is evident from the observation after implantation (Fig. 14(d)), the HAp coating consisted of two layers: a 1 μm dense inner layer and a 1 μm porous outer layer with needle-shape crystals. Before implantation, high magnification SEM observation was not carried out to identify the needle-shape crystals, in order to avoid the damage in the coating by electron beam irradiation since the samples observed by SEM were used for the implantation tests. The surface morphology of the HAp coating is similar to those formed on WE43 and pure Mg disks and on MgCa and pure Mg rods coated under the same conditions [32, 37, 42]. To show the detailed coating structures, the surface and cross-sectional SEM images of CAp and HAp coatings

formed on the pure Mg disks is shown in Fig. S1 in the supplementary materials. Figure S1 shows that the CAp coating is a single layer of about 1 μm thick consisting of agglomerated particles, while the HAp coating is a two-layer structure with an inner layer of about 1 μm thick and an outer layer of about 1 μm thick consisting of needle-shape crystals.

Table 2 shows the composition and the Ca/P and (Ca+Na+K)/P ratios in CAp and HAp coatings determined using EDS. The CAp-coated and HAp-coated surfaces showed the presence of C, O, Mg, Ca, P and small amount of Na and K. In CAp, Ca sites are easily substituted for Na to compensate for the difference in valence between $PO_4^{3-}$ and $CO_3^{2-}$. It was reported that small amount of Na, K and Mg was incorporated in the crystal structure of the HAp coatings of pure Mg and MgCa disks [37,42]. Meanwhile, in this result, the majority of Mg detected by EDS was derived from substrate alloy, so that the (Ca+Na+K)/P ratio was obtained. In Table 2, the composition on the CAp or HAp coating appears to be different between the screw and the plate, However, this is presumably because the severe unevenness of the screw surface and insufficient conductivity of between the screw and the sample stage prevented the accurate EDS analysis. Thus, the differences in values between plate and screw were not regarded as significant differences. There was no significant difference in the Ca/P ratio between CAp and HAp coatings, while the (Ca+Na+K)/P ratio of the CAp coatings was higher than that of the HAp coatings. These results indicate that a part of phosphate group in apatite was replaced with carbonate group in the CAp coatings.

Figure 4(a) and (b) shows the wide-range XRD patterns of the CAp-coated and HAp-coated plates and screws. It should be noted that the obtained positions of the diffraction peaks are not exactly accurate since the surface of plates and screws is not flat. Especially for screws, XRD measurement could not be done properly on the low

and high angle side due to the severe unevenness. The wide-range XRD patterns show diffraction peaks around 26, 28.5, 40.5, 46, 49.5, 52.5 and 53 degrees which are derived from apatite structure (#00-009-0432), in addition to peaks around 31, 32, 34, 36.5 and 48 degrees which are derived from substrate MgCa alloy. This result shows that apatite was formed on the CAp-coated and HAp-coated plates and screws.

Figure 4(c) and (d) shows the magnified diffraction peak from 002 plane of apatite. The position of 002 plane peak of the CAp coatings was on the lower angle side than that of the HAp coatings, and that of the CAp and HAp coatings of the plate was about 25.76 degrees and 25.93 degrees, respectively (Fig. 4(c)). This peak shift indicates the formation of B-type CAp in which phosphate group is replaced by carbonate group [32].

Figure 5 shows the FTIR spectra of the CAp-coated and HAp-coated plates and screws. The HAp-coated plates and screws exhibited absorption peaks at around 560, 600, 960, 1010, 1085 $cm^{-1}$ derived from $PO_4^{3-}$ and $HPO_4^{2-}$, a broad peak around 3600 $cm^{-1}$ attributed to $H_2O$ and a tiny peak at 3570 $cm^{-1}$ derived from $OH^-$ [43-46]. Additionally, a small peak around 1650 $cm^{-1}$ derived from $CO_3^{2-}$ was observed. The CAp-coated plate and screw exhibited absorption peaks at 871, 1420, 1475 and 1650 $cm^{-1}$ derived from $CO_3^{2-}$ [43-46], in addition to the peaks derived from $PO_4^{3-}$, $HPO_4^{2-}$, $H_2O$ and $OH^-$, similar to the HAp-coated device. The clear appearance of the $CO_3^{2-}$ absorption peaks on the CAp-coated device confirms the replacement of phosphate group by carbonate group in the apatite structure [39].

### *3.2. X-ray photographs of femurs with MgCa devices with and without CAp and HAp coatings*

Figure 6 shows the X-ray photographs of femurs with CAp-coated, HAp-coated and uncoated MgCa devices implanted. At 1 week, the uncoated devices showed a relatively

large gas cavity over the plate indicated by an arrow. The size of gas cavities apparently decreased by 4 weeks and became gradually covered by new bone to be almost completely covered by 18 weeks. The initial gas cavity formation was clearly suppressed with the CAp and HAp coatings, except small cavities around screw heads probably due to the initial damage. The HAp-coated plates showed gas cavities over the plate after 8 weeks. The new bone formation over plate was not clear for the CAp-coated and HAp-coated devices in comparison to that for the uncoated devices.

### *3.3. Low magnification X-ray μCT, TB-stained and SEM images of femurs with plates and screws with and without CAp and HAp coatings*

Figures 7, 8 and 9 show the μCT, TB-stained and SEM longitudinal cross-sectional images of femurs with the CAp-coated, HAp-coated and uncoated MgCa devices implanted for 8 and 24 weeks. The μCT images of transverse cross-sectioned screws and sliced plates at a depth of about 200 μm from both side surfaces are also shown in Fig. 7. The SEM images of all three samples are shown Figs. S2 and S3 in the supplementary materials.

First, corrosion morphology of the MgCa plates and screws was observed. At 8 weeks, no obvious difference in corrosion morphology was observed either between CAp-coated and HAp-coated devices or between surrounding tissue types (Figs. 7-9). The apatite-coated devices showed corrosion pits of a few tens of micrometers deep in places and screw threads were preferentially corroded, while the original shape of each device was almost retained. The uncoated devices had thinned and corrosion pits deeper than those of the apatite-coated devices were formed. Despite the apatite coatings, cavities formed in the bone marrow, with the total volume of cavities apparently being larger around uncoated screws compared to apatite-coated screws (Fig. 8).

Up to 24 weeks, the effect of the apatite coatings on the corrosion morphology became clear. On the CAp-coated devices, the surface level was not clearly reduced on most surfaces and the corrosion progress was relatively small in the areas where new bone adhered, while corrosion pits of around 500 μm depth were formed in places on the bone side of the plate and screw. Almost the entire surface of the HAp-coated devices had thinned, and large corrosion pits of about 1 mm depth were formed on the screws. The corrosion pits were formed on both sides of the HAp-coated plates. The uncoated devices had clearly thinned by the corrosion progress and the dissolution of $Mg(OH)_2$, which decreased the fixation of the screws to the cortical bone. The volume of cavities in the bone marrow increased around the CAp-coated and HAp-coated screws in comparison to the 8th week. The large corrosion pits were formed preferentially on the bone side of the uncoated plate. However, it should be noted that the corrosion morphology showed large variation between the respective samples, indicating numerous factors such as damage during surgery, distance to bone, and initial fixation affected the corrosion morphology.

The effect of apatite coatings on the corrosion rate was then examined. The ratio of the remaining uncorroded area to the original area is shown in Fig. 10(a) and (b). The mean corrosion thinning rate for 0-8 and 0-24 weeks is shown in Fig. 10(c) and (d). In the case of plates, at 8 weeks, the CAp-coated and HAp-coated plates showed about 5% cross-sectional area reduction, as the rate of remaining cross-sectional area to original area is about 0.95 (Fig. 10(a)). Similarly, the uncoated plates showed about 20% area reduction (Fig. 10(a)). Afterwords, the CAp-coated plates did not show apparent further area reduction. On the contrary, the area reduction of the HAp-coated plates continued to show about 20% at 24 weeks. The area reduction of the uncoated plates continued monotonously to show about 45% by the 24th weeks. In the case of screws, at 8 weeks,

the similar area reduction of about 20% was shown regardless of the apatite coating, indicating that the damage during surgery was dominant. After 8 weeks, the CAp-coated screws showed small area reduction, while the HAp-coated and uncoated screws showed further reduction to about 50% at 24 weeks.

The mean corrosion rate for 0-24 weeks of the CAp-coated plates and screws was about 1/5 and 1/2 of those of the uncoated ones, respectively. That of the HAp-coated plates and screws was about 1/2 and 1 time that of the uncoated ones, respectively. The mean corrosion rate for 0-24 weeks of the CAp-coated plates and screws was less than half of that of the HAp-coated ones, indicating that the corrosion suppression ability of the CAp coating was more than twice that of the HAp coating. The corrosion rate of the screws was higher than that of the plates regardless of the apatite coatings, which is due to the screws sustaining more surgical damage compared to the plates, such as chipping of the screw heads and breaking of the coatings due to abrasion against bone and tools.

Then, the bone formation behavior was observed. The total bone contact length of screws obtained from the μCT images of transverse cross-sectioned screws is shown in Fig. 11. By the 8th week, new bone grew from the cortical bone to the surface of both CAp-coated and HAp-coated screws as if avoiding gas bubbles. However, such bone growth was not apparently observed around the uncoated screw. In the bone marrow, porous new bone formed around HAp-coated and uncoated screw, as well as along the inner surface of the cortical bone with the uncoated screws. The transverse section μCT images of apatite-coated screws show that new bone formation occurred not only from the cut surface but also from the inner wall of the cortical bone. As shown in Fig. 11, the bone contact length for CAp-coated and HAp-coated screws was relatively longer than that for uncoated screws, although statistically significant difference was not shown. By the 24th week, the bone contact length increased on CAp-coated and HAp-

coated screw surfaces as shown in Fig. 11. In contrast, only little new bone formation was observed on uncoated surfaces. At 24th weeks, the cortical bone facing to the CAp-coated plates was thickened but became porous, while the cortical bone facing to the HAp-coated and uncoated plates became porous and thinned.

As shown in the following, bone formation was also observed away from the cortical bone. Porous new bone formation is observed over the soft tissue side of the plates as if avoiding gas bubbles especially for the uncoated plates from 8 weeks (Fig. 7-9). The porous new bone formation over the CAp-coated and HAp-coated plates occurred later than for the uncoated plate. The distance between the porous new bone and the plate was about 0.5 mm for the CAp-coated plates, about 1.5 mm for the HAp-coated plates and about 2 mm for the uncoated plates on the SEM images (Fig. 9).

### *3.4. High magnification SEM images near the surface of plates and screws with and without CAp and HAp coatings*

Figure 12 shows the magnified SEM images of the near surface areas of the CAp-coated, HAp-coated and uncoated plates marked with *1 and *2 in Fig. 9. Figure 13 shows the magnified SEM images of the near surface areas of the screws marked with #1 and #2 in Fig. 9. The CAp-coated plates showed a relatively uniform corrosion layer of 5-50 μm thickness consisting of $Mg(OH)_2$ under the coating at 8 weeks (Fig. 9 and 12(a)), and no obvious corrosion progress was observed at 24 weeks (Fig. 12(b)). The HAp-coated plates showed a uniform $Mg(OH)_2$ layer similarly to the CAp-coated plates at 8 weeks. Afterwards, the corrosion of MgCa substrate and the dissolution of $Mg(OH)_2$ layer progressed with breaking the HAp coating, and a calcium phosphate layer was sometimes formed on the $Mg(OH)_2$ layer as shown in Fig. 12(d)-(1). The uncoated plates showed a uniform $Mg(OH)_2$ layer of about 50 μm thickness at 8 weeks

(Fig. 12(e)). Additionally, a calcium phosphate layer of about 1 μm and about 50 μm thick were sometimes formed on the $Mg(OH)_2$ layer of the soft-tissue and bone sides, respectively (Fig. 12(e)), and new bone formation was observed preferentially on the calcium phosphate layer (Fig. 12(f)). Dissolution of $Mg(OH)_2$ could increase the surrounding pH, leading to calcium phosphate deposition.

### *3.5. Degradation behavior of CAp and HAp coatings*

Figure 14 shows the highly magnified SEM images of the CAp and HAp coatings at the boundary between the cortical bone and the screw and in the bone marrow encircled on Fig. 13. Composition of spots A-E on Fig. 14(b)-(1-2) of the CAp-coated screw is shown in Table 3. At 8 weeks, most of the CAp coatings almost retained the original morphology on the plate and screw surfaces (Figs. 12-14(a)); whereas, preferentially on the soft tissue side of the plates, the CAp coatings were broken by a few to tens of micrometers where $Mg(OH)_2$ was slightly dissolved (Fig. 12(a)-(1)). At 24 weeks on the plates, the low magnification SEM images (Fig. 9) show that the CAp coating was not found in relatively deep localized corrosion areas. On the screws, the CAp coating was swollen to about 5 μm thickness between the cortical bone and the $Mg(OH)_2$ layer (Fig. 14(b)-(1)) and dissolved at the boundary between the adhered new bone and the $Mg(OH)_2$ layer (Fig. 14(b)-(2)). The concentration of Ca and P on the spots A-C on the swollen CAp coating was lower than that on the spot E of bone. The Ca/P ratio of the spots A-C was 1.29-1.65 that is higher than that of the as-prepared CAp coating (Table 2) and close to that of bone. These results indicate that the CAp coating began dissolving and being replaced by bone.

The HAp coating almost retained the original morphology as needle-like HAp crystals in the outer layer was observed at 24 weeks (Fig. 14(d)). On the other hand, the

magnified SEM images show that the HAp coating was not found in relatively large corrosion pits (Fig. 12(c) and (d)). This indicates that the HAp coating in large corrosion pits had been fragmented to disperse elsewhere or had been dissolved in the high pH environment.

The uncoated plates and screws showed the formation of a calcium phosphate layer on the $Mg(OH)_2$ layer with the progress of corrosion, while a thin calcium phosphate layer sometimes showed breakage where the $Mg(OH)_2$ layer was significantly dissolved (Fig. 12(e)-(1)).

### *3.6. Histological observation of the surrounding tissues*

Figure 15 shows the magnified TB-stained longitudinal cross-sectional images of the boundary between the cortical bone and the CAp-coated, HAp-coated and uncoated screws implanted for 8 and 24 weeks. Black substance is MgCa metal and blue-stained amorphous-like substance on the metal surface is corrosion product of $Mg(OH)_2$ according to the results of SEM-EDS observation.

New bone formed on the apatite-coated surfaces contained cells in the vicinity of the coating surface regardless of the corrosion progress under the coatings at 8 and 24 weeks. There was no significant difference in the number of cells in the vicinity of the CAp and HAp coatings. However, cells were absent in the new and original bone that was in direct contact with the corrosion products. The uncoated surface closely contacted to the original bone, but new bone was not formed at the boundary at 8 weeks. At 24 weeks, new bone was formed on the corrosion product layer of the uncoated surface, but there were much fewer number of cells being present in the vicinity of the screw surface in comparison to the apatite-coated surfaces.

The higher magnification SEM image of the CAp-coated screw at 24 weeks (Fig. 15(b)-(2)) shows that there was an unstained substance layer with several micrometers thickness between the new bone and the corrosion product, which is presumed to be the swollen CAp coating.

Figure 16 shows the HE-stained transverse cross-sectional images of the femurs with the CAp-coated, HAp-coated and uncoated screws and the magnified images of the boundary between the bone and the screw implanted for 8 and 24 weeks. Around the uncoated devices, abscess formation was observed as indicated by arrows at 8 weeks (Fig. 16(e)), and it was hardly observed at 24 weeks. Such abscess formation was not observed around the CAp-coated and HAp-coated devices for 24 weeks. The magnified images of the boundary between the bone and the screw show that there was not multinucleated cell like osteoclast in the vicinity of the CAp and HAp coatings.

## 4. Discussion

### *4.1. CAp and HAp coating of MgCa plates and screws*

The optical and SEM observations demonstrated that uniform CAp and HAp coatings can be formed on the highly uneven MgCa plate and screw surfaces with morphologies and thicknesses similar to those conventionally formed on WE43 and pure Mg disks as well as MgCa rods [30, 33, 37]. It was demonstrated that the developed coating method is effective in forming uniform CAp and HAp coatings on Mg alloy devices with highly uneven surfaces, such as mesh plates and porous materials, regardless of substrate surface topography.

The approximate carbonate content in the CAp coating of plates was estimated to be about 20wt% based on the 002 plane peak position of 25.76 degrees, using the

previously reported method [43, 47]. This carbonate content is comparable to 10-20wt% of bone apatite in the human body [47].

### *4.2. Effect of CAp and HAp coatings on corrosion behavior of substrate MgCa alloy*

During the initial stage of implantation, the corrosion suppression effect of the HAp and CAp coatings on MgCa corrosion was equivalent, and the corrosion morphology did not depend on the presence of the apatite coatings or on the type of the surrounding tissue (Fig. 9 and 10). The corrosion suppression effect of the CAp coating should have increased from 8 to 24 weeks as shown by the decrease in the corrosion rate (Fig. 10). This improvement may be attributed to the repair of initial coating defects and the corrosion suppression ability of the $Mg(OH)_2$ corrosion product layer. In contrast, the corrosion suppression ability of the HAp coating decreased locally to show millimeter size pits. As the result, the corrosion suppression ability of the CAp coating became about 2 times higher than that of the HAp coating. Similar long-term superior corrosion suppression ability of the CAp coating over the HAp coating was observed for WE43 in a culture medium [40]. These results demonstrated that the mechanical integrity of MgCa screws can be improved with CAp and HAp coatings. This improved mechanical integrity continues for a long period of time for CAp-coated screws, which exhibit small, uniform corrosion, whereas HAp-coated screws lose mechanical integrity due to the formation of millimeter-sized corrosion pits.

Kim et al. reported that uncoated pure Mg screws showed a degradation volume of about 35% in rabbit tibial shaft for 12 weeks, whereas 2 h-treated HAp coating reduced the degradation volume to about 25% [18]. Cheng et al. reported that the 12 h-treated HAp-coated pure Mg rod showed only a slight corrosion in rat femur at 8 weeks [24].

These HAp coating performance in corrosion is better than that of the 1 h-treated CAp-coated MgCa screws in this study. Moreover, large corrosion pits were not observed on 2 h-treated HAp-coated pure Mg screws [18] or on 12 h-treated HAp-coated pure Mg rod [24]. These facts indicate that the performance of the HAp-coated MgCa can be improved with increasing coating treatment period.

The substrate MgCa alloy formed a $Mg(OH)_2$ layer on the corroded surface, which gradually dissolved with time (Figs. 7-9). Occasionally, a dense calcium phosphate layer formed on the $Mg(OH)_2$ layer, indicating that the dissolution of $Mg(OH)_2$ raised the surrounding pH and led to calcium phosphate deposition from body fluids. Additionally, the localized dissolution of $Mg(OH)_2$ at micrometer level occurred (Fig. 12(a), (c) and (e)), indicating that the niche environment created by cell adhesion and other factors influences Mg alloy corrosion.

Between plates and screws, the screws showed a higher cross-sectional reduction rate through 24 weeks (Fig. 10(c) and (d)), likely due to the plentiful blood flow in the bone marrow. Meanwhile, the plate surface area in contact with body fluid might decrease as it was covered by soft tissue, surrounded by $H_2$ gas bubbles due to corrosion, or covered by new bone, which presumably decrease the corrosion rate.

### *4.3. Degradation behavior of CAp and HAp coatings*

By the 8th week, the CAp and HAp coatings almost retained their original morphology on most of the surfaces. However, in a few regions, the apatite coatings exhibited microscopic damage where the $Mg(OH)_2$ layer had dissolved. This phenomenon can be attributed the increased solubility of HAp at a pH above 9 [48] and the fact that the pH of a saturated $Mg(OH)_2$ solution is 10.5. Zhang et al. reported that macrophage cells phagocytose corrosion products of Mg-Nd-Zn-Zr alloy, which

consisted of $Mg(OH)_2$ and calcium and magnesium phosphate compounds [49]. This phagocytosis by macrophage cells may also be responsible for localized dissolution of the apatite coatings.

At 24 weeks, the CAp coating, on which new bone had formed during the early stage, exhibited swelling (Fig. 14). Notably, the CAp coating of WE43 showed degradation beneath osteoclast cell bodies in cell culture tests [32], suggesting that osteoclast cells can dissolve the developed CAp coatings. However, the histological observation revealed that osteoclast cells were scarce in the vicinity of the CAp coating (Figs. 15 and 16). The presence of multinucleated cells like osteoclasts were also not pronounced around CAp blocks implanted in dog mandible bones for 4 and 12 weeks, the but CAp was largely dissolved, while vigorous new bone formation was observed on the surface of the CAp [39], indicating that the involvement of osteoclasts in CAp coating dissolution cannot be denied just because no osteoclasts are observed. On the other hand, as previously mentioned, both the CAp and HAp coatings dissolved in the areas where the $Mg(OH)_2$ layer had dissolved (Fig. 12). The early born formation seems to play a role in the dissolution of the CAp coating (Fig. 14), suggesting that the pH increase around the apatite coatings due to $Mg(OH)_2$ dissolution is further enhanced by mass transfer inhibition due to adhered bone. Generally, the solubility of CAp is higher than that of HAp [50]. The CAp coating was possibly chemically dissolved. However, further investigation is necessary to understand the in vivo dissolution of CAp coatings of Mg alloy.

Neither TB-stained nor HE-stained images showed inflammatory cell infiltrates in the vicinity of the CAp coatings (Figs. 15 and 16). Ishikawa et al. reported that CAp blocks showed the weakest inflammatory cell infiltration in the surrounding bone tissue

compared to HAp and β-TCP blocks [39]. Therefore, no adverse effect of CAp coating dissolution on bone tissue is expected.

### *4.4. Bone formation behavior on and distance from CAp-coated and HAp-coated MgCa plate and screw*

Around the devices with and without apatite coatings, the new bone grew from the cortical bone toward the screw surface first and proliferated on the screw surface. This behavior indicates that the bone formation on the device surface depends not only on the surface properties of devices but also on the distance between the bone and the device. This could explain why no statistically significant difference in the bone contact length of the screws, with or without apatite coatings, was observed in Fig. 11. Meanwhile, both the CAp and HAp coatings tended to enhance the bone formation on their surfaces, consistent with previous findings [32, 37]. There was no apparent difference in the bone contact length between the CAp-coated and HAp-coated screws at 8 weeks, indicating their comparable bone formation ability. This result is consistent with the previous result that the CAp and HAp coatings of WE43 enhanced the alkaline phosphatase (ALP) expression level from MC3T3-E1 osteoblast cells to the comparable extent at 3 weeks [32]. Additionally, the HAp coatings of Mg alloys were reported to exhibit high osteoconductivity [24, 37], while bulk CAp demonstrated high bone formation ability [39].

For the CAp-coated screws, the bone contact length increased with time, the corrosion was uniform, and the degree of porosity in the cortical bone was relatively low (Figs 7-9), maintaining the bone-screw bonding for 24 weeks. In contrast, the HAp-coated screws showed the apparent increase in bone contact length (Fig. 11), but the

screws' fixation deteriorated due to the large corrosion pits and the cortical bone becoming porous (Fig. 7-9).

Besides the new bone formation on the device surface, there was another new bone formation at a distance from the device surface, such as that over the plates. This bone formation was presumably induced by pH increase and $Mg^{2+}$ ions resulting from MgCa corrosion. This is because weak alkaline conditions stimulated the osteoblast differentiation and suppressed the osteoclast formation [51], the proliferation and ALP activity of osteoblasts were enhanced at pH>8 [52], and the osteoclastic activities were suppressed in alkaline environments containing $Mg^{2+}$ ions [53]. On the other hand, excess pH increase and too high $Mg^{2+}$ ion concentration do not enhance the bone formation, because osteoblast and osteoclast activity depends on $Mg^{2+}$ ion concentration and the osteoblast cells could die on the corrosion pits formed under the HAp coating of Mg alloy [54, 55]. The distance between the plate surface and the porous bone was greater for the uncoated plates with larger corrosion compared to the CAp-coated plates with smaller corrosion (Figs. 7 and 9). These facts indicate that a suitable pH and $Mg^{2+}$ ion concentration environment for the bone formation was formed some distance from the MgCa devices.

Around the uncoated MgCa devices, the new bone formation over the plates was initially more pronounced than that at the boundary between the cortical bone and the screw, due to the rapid corrosion which could disturb the cell adhesion. As the entire surface became covered with the $Mg(OH)_2$ layer (Figs. 7-9), the bone formation on the uncoated MgCa surface remarkably increased, especially on the calcium phosphate layer on the $Mg(OH)_2$ layer.

The influence of the apatite coatings was also observed on the cortical bone facing to the MgCa devices, which became porous with time (Figs. 7-9). The porosity of the

cortical bone facing the CAp-coated devices was lower than that facing the HAp-coated devices and notably lower than that facing the uncoated MgCa devices. Micro-pore formation in the cortical bone occurred later than the MgCa corrosion in rat femurs with the HAp-coated MgCa rods [37], suggesting that the pH increase due to the MgCa corrosion played a role in the micro-pore formation in the cortical bone. Particularly for the uncoated devices, the gas cavities between the plates and cortical bone have prevented body fluids from contacting the cortical bone for long period of time, possibly causing the cortical bone to be thinned and porous. Further investigation is needed to understand the effect of Mg alloy corrosion on the surrounding bone.

## 5. Conclusions

The degradation behavior of the CAp-coated and HAp-coated MgCa plates and screws and the bone formation behavior around the devices were investigated in rabbit femurs. Findings are summarized below:

1) The CAp and HAp coatings were uniformly applied to the uneven surfaces of the MgCa plates and screws using the developed coating treatment.

2) The CAp coating reduced the mean corrosion rate of MgCa devices to about 1/5, and the HAp coating to about 1/2, compared to the uncoated devices after 24 weeks. This demonstrates that the CAp coating had twice the corrosion suppression effect of the HAp coating.

3) The HAp-coated devices exhibited significant localized corrosion, while the CAp-coated devices exhibited nearly uniform corrosion.

4) The CAp coating began dissolving by 24 weeks, while the HAp coating retained its shape.

5) Both CAp and HAp coatings promoted bone formation approximately twice as much as that of the uncoated devices.

6) The uncoated devices showed slight abscess formation, whereas the CAp and HAp coatings suppressed abscess formation near the device surface.

Both CAp and HAp coatings demonstrated beneficial properties by suppressing corrosion and promoting bone formation in MgCa devices, making them promising for biodegradable Mg alloy devices. Additionally, the CAp coating showed superior corrosion suppression and had the characteristic of dissolving over time. This study demonstrated clinically viable options of bioabsorbable and non-absorbable coatings for biodegradable Mg alloys. The choice of Mg alloy coating should depend on the treatment purpose and application area, offering targeted and versatile solutions for clinical applications.

**Acknowledgements**

We would like to thank Ms. E. Ikeda of NIMS for her through experimental support. The FTIR measurement was supported by the NIMS Molecule & Material Synthesis Platform in the Nanotechnology Platform Project.

**Declarations**

The animal experiments were approved with the approval number D20008 by the Institutional Animal Experiment Committee of Kagoshima University in Japan. Informed consent was not obtained because no experiments were performed on human subjects. This work was mostly supported by JSPS Grant-in-Aid for Scientific Research (C) Grant Number 20K10012 and partially supported by JSPS KAKENHI Grant Number 22H01798. The authors have no competing interests to declare that are relevant

to the content of this article.

**Data Availability**

The data that support the findings of this study are available from the corresponding author, [S.H.], upon reasonable request.

**References**

1. Witte, F.: The history of biodegradable magnesium implants: A review. Acta Biomater. 6(5), 1680-92 (2010). doi: 10.1016/j.actbio.2010.02.028.

2. Zeng, R.C., Dietzel, W., Witte, F., Hort, N., Blawert, C.: Progress and Challenge for Magnesium Alloys as Biomaterials. Adv Biomater. 10(8), B3-B14 (2008). doi: 10.1002/adem.200800035.

3. Zhao, D., Witte, F., Lu, F., Wang, J., Li, J., Qin, L.: Current status on clinical applications of magnesium-based orthopaedic implants: A review from clinical translational perspective. Biomaterials. 112, 287-302 (2017). doi: 10.1016/j.biomaterials.2016.10.017.

4. Kuwahara, H., Al-Abdullat, Y., Mazaki, N., Tsutsumi, S., Aizawa, T.: Precipitation of magnesium apatite on pure magnesium surface during immersing in Hank's solution. Mater Trans. 42(7), 1317-21 (2001). doi: 10.2320/matertrans.42.1317.

5. Hornberger, H., Virtanen, S., Boccaccini, A.R.: Biomedical coatings on magnesium alloys - A review. Acta Biomater. 8(7), 2442-55 (2012). doi: 10.1016/j.actbio.2012.04.012.

6. Treiser, M., Abramson, S., Langer, R., Kohn, J. Degradable and Resorbable Biomaterials. In: Ratner BD, Hoffman AS, Schoen FJ, Lemons JE, editors. Biomaterials Science: An Introduction to Materials in Medicine Third Edition. 3rd Edition ed. MA, USA: Elsevier; 2013. p. 179-95.

7. Plaass, C., Ettinger, S., Sonnow, L., Koenneker, S., Noll, Y., Weizbauer, A., et al.: Early results using a biodegradable magnesium screw for modified chevron osteotomies. J Orthop Res. 34(12), 2207-14 (2016). doi: 10.1002/jor.23241.

8. Haude, M., Ince, H., Kische, S., Abizaid, A., Tolg, R., Alves Lemos, P., et al.: Sustained safety and clinical performance of a drug-eluting absorbable metal scaffold

up to 24 months: pooled outcomes of BIOSOLVE-II and BIOSOLVE-III. EuroIntervention. 13(4), 432-9 (2017). doi: 10.4244/EIJ-D-17-00254.
9. Haude, M., Erbel, R., Erne, P., Verheye, S., Degen, H., Bose, D., et al.: Safety and performance of the drug-eluting absorbable metal scaffold (DREAMS) in patients with de-novo coronary lesions: 12 month results ofthe prospective, multicentre, first-in-man BIOSOLVE-I trial. Lancet. 381(9869), 836-44 (2013). doi: 10. 1016/S0140-6736(12)61765-6.
10. Seitz, J.M., Lucas, A., Kirschner, M.: Magnesium-Based Compression Screws: A Novelty in the Clinical Use of Implants. Jom. 68(4), 1177-82 (2016). doi: 10.1007/s11837-015-1773-1.
11. Joner, M., Ruppelt, P., Zumstein, P., Lapointe-Corriveau, C., Leclerc, G., Bulin, A., et al.: Preclinical Evaluation of Degradation Kinetics and Elemental Mapping of First and Second Generation Bioresorbable Magnesium Scaffolds. EuroIntervention. 14(9), e1040-e8 (2018). doi: 10.4244/EIJ-D-17-00708.
12. Waksman, R., Zumstein, P., Pritsch, M., Wittchow, E., Haude, M., Lapointe-Corriveau, C., et al.: Second-generation magnesium scaffold Magmaris: device design and preclinical evaluation in a porcine coronary artery model. EuroIntervention. 13(4), 440-9 (2017). doi: 10.4244/EIJ-D-16-00915.
13. Byun, S.H., Lim, H.K., Cheon, K.H., Lee, S.M., Kim, H.E., Lee, J.H.: Biodegradable magnesium alloy (WE43) in bone-fixation plate and screw. Journal of biomedical materials research Part B, Applied biomaterials. 108B, 2505-12 (2020). doi: 10.1002/jbm.b.34582.
14. Naujokat, H., Seitz, J.M., Acil, Y., Damm, T., Moller, I., Gulses, A., et al.: Osteosynthesis of a cranio-osteoplasty with a biodegradable magnesium plate system in miniature pigs. Acta Biomater. 62, 434-45 (2017). doi: 10.1016/j.actbio.2017.08.031.
15. Plaass, C., von Falck, C., Ettinger, S., Sonnow, L., Calderone, F., Weizbauer, A., et al.: Bioabsorbable magnesium versus standard titanium compression screws for fixation of distal metatarsal osteotomies - 3 year results of a randomized clinical trial. J Orthop Sci. 23(2), 321-7 (2018). doi: 10.1016/j.jos.2017.11.005.
16. Hiromoto, S., Shishido, T., Yamamoto, A., Maruyama, N., Somekawa, H., Mukai, T.: Precipitation control of calcium phosphate on pure magnesium by anodization. Corros Sci. 50(10), 2906-13 (2008). doi: DOI 10.1016/j.corsci.2008.08.013.

17. Chai, H., Guo, L., Wang, X., Gao, X., Liu, K., Fu, Y., et al.: In vitro and in vivo evaluations on osteogenesis and biodegradability of a b-tricalcium phosphate coated magnesium alloy. J Biomed Mater Res A. 100A, 293-304 (2012).
18. Kim, S.M., Jo, J.H., Lee, S.M., Kang, M.H., Kim, H.E., Estrin, Y., et al.: Hydroxyapatite-coated magnesium implants with improved in vitro and in vivo biocorrosion, biocompatibility, and bone response. J Biomed Mater Res A. 102(2), 429-41 (2014). doi: 10.1002/jbm.a.34718.
19. Li, L., Zhang, M., Li, Y., Zhao, J., Qin, L., Lai, Y.X.: Corrosion and biocompatibility improvement of magnesium-based alloys as bone implant materials: a review. Regenerative Biomaterials. 4(2), 129-37 (2017). doi: 10.1093/rb/rbx004.
20. Jafari, S., Raman, R.K.S.: In-vitro biodegradation and corrosion-assisted cracking of a coated magnesium alloy in modified-simulated body fluid. Mater Sci Eng C-Mater Biolog Appl. 78, 278-87 (2017). doi: 10.1016/j.msec.2017.04.079.
21. Sankar, M., Suwas, S., Balasubramanian, S., Manivasagam, G.: Comparison of electrochemical behavior of hydroxyapatite coated onto WE43 Mg alloy by electrophoretic and pulsed laser deposition. Surf Coat Tech. 309, 840-8 (2017). doi: 10.1016/j.surfcoat.2016.10.077.
22. Liu, C.N., Boke, F., Gebhard, M., Devi, A., Fischer, H., Keller, A., et al.: Ultrasound-mediated deposition and cytocompatibility of apatite-like coatings on magnesium alloys. Surf Coat Tech. 345, 167-76 (2018). doi: 10.1016/j.surfcoat.2018.03.100.
23. Kamrani, S., Fleck, C.: Biodegradable magnesium alloys as temporary orthopaedic implants: a review. Biometals. 32(2), 185-93 (2019). doi: 10.1007/s10534-019-00170-y.
24. Cheng, S., Wang, W., Wang, D., Li, B., Zhou, J., Zhang, D., et al.: An in vitro and in vivo comparison of Mg(OH)2-, MgF2- and HA-coated Mg in degradation and osteointegration. Biomater Sci. 8(12), 3320-33 (2020). doi: 10.1039/d0bm00467g.
25. Sekar, P., Narendranath, S., Desai, V.: Recent progress in in vivo studies and clinical applications of magnesium based biodegradable implants - A review. Journal of Magnesium and Alloys. 9(4), 1147-63 (2021). doi: 10.1016/j.jma.2020.11.001.
26. Kacarevic, Z.P., Rider, P., Elad, A., Tadic, D., Rothamel, D., Sauer, G., et al.: Biodegradable magnesium fixation screw for barrier membranes used in guided bone regeneration. Bioact Mater. 14(8), 15-30 (2022). doi: 10.1016/j.bioactmat.2021.10.036.

27. Jana, A., Das, M., Balla, V.K.: In vitro and in vivo degradation assessment and preventive measures of biodegradable Mg alloys for biomedical applications. J Biomed Mater Res A. 110(2), 462-87 (2022). doi: 10.1002/jbm.a.37297.
28. Park, J., Um, S.H., Seo, Y., Lee, J., Kim, Y.C., Ok, M.R., et al.: Improving hydroxyapatite coating ability on biodegradable metal through laser-induced hydrothermal coating in liquid precursor: Application in orthopedic implants. Bioactive Materials. 25, 796-806 (2023). doi: 10.1016/j.bioactmat.2022.06.020.
29. Hiromoto, S.: High corrosion resistance of magnesium coated with hydroxyapatite directly synthesized in an aqueous solution. Electrochim Acta. 54(27), 7085-93 (2009). doi: 10.1016/j.electacta.2009.07.033.
30. Tomozawa, M., Hiromoto, S.: Microstructure of hydroxyapatite- and octacalcium phosphate-coatings formed on magnesium by a hydrothermal treatment at various pH values. Acta Mater. 59(1), 355-63 (2011). doi: 10.1016/j.actamat.2010.09.041.
31. Hiromoto, S., Inoue, M., Taguchi, T., Yamane, M., Ohtsu, N.: In vitro and in vivo biocompatibility and corrosion behaviour of a bioabsorbable magnesium alloy coated with octacalcium phosphate and hydroxyapatite. Acta Biomater. 11, 520-30 (2015). doi: 10.1016/j.actbio.2014.09.026.
32. Hiromoto, S., Itoh, S., Noda, N., Yamazaki, T., Katayama, H., Akashi, T.: Osteoclast and osteoblast responsive carbonate apatite coatings for biodegradable magnesium alloys. Science and Technology of Advanced Materials. 21(1), 346–58 (2020). doi: 10.1080/14686996.2020.1761237.
33. Midorikawa, K., Hiromoto, S., Yamamoto, T.: Carbonate content control in carbonate apatite coatings of biodegradable magnesium. Ceramics International. 50(4), 6784-92 (2024). doi: 10.1016/j.ceramint.2023.12.021.
34. Kasuga, T. Coatings for metallic biomaterials. In: Niinomi M, editor. Metals for biomedical devices. Camridge(UK): Woodhead Publishing Limited; 2010. p. 260-82.
35. Kikuchi, M., Ikoma, T., Itoh, S., Matsumoto, H.N., Koyama, Y., Takakuda, K., et al.: Biomimetic synthesis of bone-like nanocomposites using the self-organization mechanism of hydroxyapatite and collagen. Composites Science and Technology. 64(6), 819-25 (2004). doi: 10.1016/j.compscitech.2003.09.002.
36. Kokubo, T., Yamaguchi, S.: Novel bioactive materials developed by simulated body fluid evaluation: Surface-modified Ti metal and its alloys. Acta Biomater. 44, 16-30 (2016). doi: 10.1016/j.actbio.2016.08.013.

37. Hiromoto, S., Nozoe, E., Hanada, K., Yoshimura, T., Shima, K., Kibe, T., et al.: In vivo degradation and bone formation behaviors of hydroxyapatite-coated Mg alloys in rat femur. Mater Sci Eng C-Mater Biolog Appl. 122, 111942 (2021). doi: ARTN 111942
10.1016/j.msec.2021.111942.
38. Ishikawa, K.: Carbonate apatite bone replacement: learn from the bone. Journal of the Ceramic Society of Japan. 127(9), 595-601 (2019). doi: 10.2109/jcersj2.19042.
39. Ishikawa, K., Miyamoto, Y., Tsuchiya, A., Hayashi, K., Tsuru, K., Ohe, G.: Physical and Histological Comparison of Hydroxyapatite, Carbonate Apatite, and beta-Tricalcium Phosphate Bone Substitutes. Materials (Basel). 11(10), (2018). doi: 10.3390/ma11101993.
40. Hiromoto, S., Itoh, S., Doi, K., Katayama, H., Akashi, T.: Short- and long-term corrosion behavior of carbonate apatite-coated Mg-4mass% Y-3mass% RE alloy in cell culture medium. Corros Sci. 200, 110222 (2022). doi: 10.1016/j.corsci.2022.110222.
41. Martinez Sanchez, A.H., Luthringer, B.J., Feyerabend, F., Willumeit, R.: Mg and Mg alloys: how comparable are in vitro and in vivo corrosion rates? A review. Acta Biomater. 13, 16-31 (2015). doi: 10.1016/j.actbio.2014.11.048.
42. Ohtsu, N., Hiromoto, S., Yamane, M., Satoh, K., Tomozawa, M.: Chemical and crystallographic characterizations of hydroxyapatite- and octacalcium phosphate-coatings on magnesium synthesized by chemical solution deposition using XPS and XRD. Surf Coat Tech. 218, 114-8 (2013). doi: 10.1016/j.surfcoat.2012.12.037.
43. LeGeros, R.Z., Tung, M.S.: Chemical stability of carbonate- and fluoride-containing apatites. Caries Res. 17(5), 419-29 (1983). doi: 10.1159/000260696.
44. Rehman, I., Bonfield, W.: Characterization of hydroxyapatite and carbonated apatite by photo acoustic FTIR spectroscopy. Journal of materials science Materials in medicine. 8(1), 1-4 (1997). doi: 10.1023/a:1018570213546.
45. Hutchens, S.A., Benson, R.S., Evans, B.R., O'Neill, H.M., Rawn, C.J.: Biomimetic synthesis of calcium-deficient hydroxyapatite in a natural hydrogel. Biomaterials. 27(26), 4661-70 (2006). doi: 10.1016/j.biomaterials.2006.04.032.
46. Kuroda, D., Moriyama, M., Ichino, R., Okido, M., Seki, A.: Formation and in Vivo Evaluation of Carbonate Apatite and Carbonate Apatite/$CaCO_3$ Composite Films Using the Thermal Substrate Method in Aqueous Solution. J Japan Inst Metals. 73(5), 346-53 (2009). doi: 10.2320/jinstmet.73.346.

47. Ohtsuka, M., Matsuda, Y.: Physicochemical Properties of Synthetic Apatite and its Application Study as Biomaterials. Journal of the Association of Materials Engneering for Resources. 4(2), 128-41 (1991). doi: 10.5188/jsmerj.4.2_128.
48. Ishikawa, K.: Bone Substitute Fabrication Based on Dissolution-Precipitation Reactions. Materials. 3(2), 1138-55 (2010). doi: 10.3390/ma3021138.
49. Zhang, J., Hiromoto, S., Yamazaki, T., Huang, H., Jia, G.Z., Li, H.Y., et al.: Macrophage phagocytosis of biomedical Mg alloy degradation products prepared by electrochemical method. Mater Sci Eng C-Mater Biolog Appl. 75, 1178-83 (2017). doi: 10.1016/j.msec.2017.02.126.
50. Koda, T., DoI, Y., Shimizu, Y., Adachi, M., Wakamatsu, N., Goto, T., et al.: Sintering of Carbonatecontaining Apatites  Dissolution Behavio Investigated with a pH stat 一. The Journal of the Japanese Society for Dental Materials and Devices. 17(3), 152-8 (1998).
51. Liu, W., Wang, T., Yang, C., Darvell, B.W., Wu, J., Lin, K., et al.: Alkaline biodegradable implants for osteoporotic bone defects--importance of microenvironment pH. Osteoporos Int. 27(1), 93-104 (2016). doi: 10.1007/s00198-015-3217-8.
52. Shen, Y., Liu, W., Lin, K., Pan, H., Darvell, B.W., Peng, S., et al.: Interfacial pH: a critical factor for osteoporotic bone regeneration. Langmuir. 27(6), 2701-8 (2011). doi: 10.1021/la104876w.
53. Wu, L., Feyerabend, F., Schilling, A.F., Willumeit-Romer, R., Luthringer, B.J.C.: Effects of extracellular magnesium extract on the proliferation and differentiation of human osteoblasts and osteoclasts in coculture. Acta Biomater. 27, 294-304 (2015). doi: 10.1016/j.actbio.2015.08.042.
54. Maradze, D., Musson, D., Zheng, Y., Cornish, J., Lewis, M., Liu, Y.: High Magnesium Corrosion Rate has an Effect on Osteoclast and Mesenchymal Stem Cell Role During Bone Remodelling. Sci Rep. 8(1), 10003 (2018). doi: 10.1038/s41598-018-28476-w.
55. Hiromoto, S., Yamazaki, T.: Micormorphological effect of calcium phosphate coating on compatibility of magnesium alloy with osteoblast. Science and Technology of Advanced Materials. 18(1), 96-109 (2017).

**Table and Figure captions**

Table 1. Composition of MgCa alloy.

Table 2. Composition of CAp and HAp coatings formed on MgCa plates and screws.

Table 3. Composition of spots marked on the SEM image of the CAp-coated screw implanted for 24 weeks shown in Fig. 13(b)-(1-2).

Figure 1. Appearance and dimensions of MgCa plates and screws.

Figure 2. Experimental procedure.

Figure 3. Optical images of (a) CAp-coated plate, (b) CAp-coated screw, (c) HAp-coated plate, and (d) HAp-coated screw. Surface SEM images of (e) CAp-coated plate, (f) CAp-coated screw, (g) HAp-coated plate, and (h) HAp-coated screw with (1) low and (2) high magnifications. (i) Cross-sectional SEM image of CAp-coated screw.

Figure 4. (a) and (b) Wide range XRD patterns and (c) and (d) magnified apatite 002 plane diffraction peak of (a) and (c) plate and (b) and (d) screw with (i) CAp and (ii) HAp coatings.

Figure 5. FTIR spectra of (a) plate and (b) screw with (i) CAp and (ii) HAp coatings.

Figure 6. X-ray photographs of femurs with (a) CAp-coated, (b) HAp-coated and (c) uncoated devices implanted for 1, 4, 8, 12, 18 and 24 weeks.

Figure 7. X-ray μCT images of (a)-(f) longitudinally sectioned femurs with plates and screws, (g)-(l) transversely sectioned femur with screw and (m)-(r) horizontally sliced plates, implanted for 8 and 24 weeks. (a), (b), (g), (h), (m) and (n) CAp-coated, (c), (d), (i), (j), (o) and (p) HAp-coated and (e), (f), (k), (l), (q) and (r) uncoated devices. Yellow substance: metal, blue substance: original bone, yellow and green substance: new bone, and dark area: gas cavity.

Figure 8. TB-stained longitudinal cross-sectional images of femurs with (a) and (b) CAp-coated, (c) and (d) HAp-coated and (e) and (f) uncoated MgCa devices implanted for (a), (c) and (e) 8 weeks and (b), (d) and (f) 24 weeks.

Figure 9. SEM images of longitudinal cross section of femurs with (a) and (b) CAp-coated, (c) and (d) HAp-coated and (e) and (f) uncoated MgCa devices implanted for (a), (c) and (e) 8 weeks and (b), (d) and (f) 24 weeks. Bright contrasting substance: metal, dark grey contrasting substance on metal: corrosion product consisting mainly of $Mg(OH)_2$, light grey contrasting substance: bone, bright contrasting dense substance on $Mg(OH)_2$ layer: calcium phosphate, and darkest contrasting substance: embedded resin, according to EDS analysis.

Figure 10. (a) and (b) Ratio of remaining cross-sectional area to original area and (c) and (d) mean corrosion rate for 8 and 24 weeks of CAp-coated, HAp-coated and uncoated (a) and (c) plate and (b) and (d) screw. n.s.: not significant, *: $p<0.05$, **: $p<0.01$.

Figure 11. Total bone contact length of MgCa screws with and without CAp and HAp coatings implanted for 8 and 24 weeks. n.s.: not significant.

Figure 12. Magnified SEM images of near surface areas on (a) and (b) CAp-coated, (c) and (d) HAp-coated and (e) and (f) uncoated plates implanted for (a), (c) and (e) 8 weeks and (b), (d) and (f) 24 weeks. (1) soft-tissue side and (2) bone sides of plate marked with *1 and *2 in Fig. 9, respectively.

Figure 13. Magnified SEM images of near surface areas on (a) and (b) CAp-coated, (c) and (d) HAp-coated and (e) and (f) uncoated screws implanted for (a), (c) and (e) 8 weeks and (b), (d) and (f) 24 weeks. (1) area between cortical bone and screw and (2) area in bone marrow of screw marked with #1 and #2 in Fig. 9, respectively.

Figure 14. Highly magnified SEM images of (a) and (b) CAp coating and (c) and (d) HAp coating (1) at boundary between cortical bone and screw and (2) in bone marrow encircled on Fig. 12, implanted for (a) and (c) 8 weeks and (b) and (d) 24 weeks.

Figure 15. Magnified TB-stained images of boundary between cortical bone and (a) and (b) CAp-coated, (c) and (d) HAp-coated and (e) and (f) uncoated screws implanted for (a), (c) and (e) 8 weeks and (b), (d) and (f) 24 weeks.

Figure 16. HE-stained transverse cross sectional images of femurs with (a) and (b) CAp-coated, (c) and (d) HAp-coated and (e) and (f) uncoated screws implanted for (a), (c) and (e) 8 weeks and (b), (d) and (f) 24 weeks. (1) Low magnification image and (2) high magnification image of the squared area on image (1). Star mark indicates where screw and plate were located.

Table 1. Composition of MgCa alloy. (mass%)

| Mg | Ca | Al | Si | Mn | Fe |
|---|---|---|---|---|---|
| Bal. | 0.8092 | 0.0039 | 0.0090 | 0.0014 | 0.0015 |

Table 2. Composition of CAp and HAp coatings formed on MgCa plates and screws.

| | CAp-coated MgCa | | HAp-coated MgCa | |
|---|---|---|---|---|
| atomic% | Plate | Screw | Plate | Screw |
| C | 11.4±0.2 | 15.9±0.5 | 8.4±0.2 | 7.0±0.4 |
| O | 33.1±1.6 | 31.7±2.7 | 45.2±1.6 | 50.1±1.3 |
| Mg | 42.5±2.3 | 40.3±3.5 | 23.8±2.3 | 15.7±1.8 |
| Ca | 5.5±0.5 | 4.8±0.6 | 10.6±0.6 | 13.5±0.9 |
| P | 4.7±0.3 | 4.2±0.4 | 9.6±0.3 | 11.0±0.5 |
| Na | 2.9±0.1 | 3.0±0.3 | 2.2±0.0 | 2.5±0.0 |
| K | 0.1±0.0 | 0.2±0.0 | 0.2±0.0 | 0.2±0.0 |
| Ca/P ratio | 1.16±0.04 | 1.13±0.03 | 1.11±0.03 | 1.23±0.03 |
| (Ca+Na+K)/P | 1.80±0.02 | 1.86±0.05 | 1.36±0.02 | 1.48±0.02 |

Table 3. Composition of spots marked on the SEM image of the CAp-coated screw implanted for 24 weeks shown in Fig. 13(b)-(1-2).

| at% | Spot A | Spot B | Spot C | Spot D | Spot E |
|---|---|---|---|---|---|
| C | 27.14 | 22.41 | 22.30 | 31.87 | 31.32 |
| O | 48.28 | 56.36 | 55.72 | 49.21 | 45.64 |
| Ca | 14.05 | 9.05 | 9.23 | 2.19 | 13.74 |
| P | 8.50 | 6.89 | 7.14 | 5.53 | 8.22 |
| Mg | 2.04 | 5.29 | 5.62 | 10.41 | 1.08 |
| Na | - | - | - | 0.79 | - |
| Ca/P ratio | 1.65 | 1.31 | 1.29 | 0.40 | 1.67 |
| (Ca+Na)/P | 1.65 | 1.31 | 1.29 | 0.54 | 1.67 |

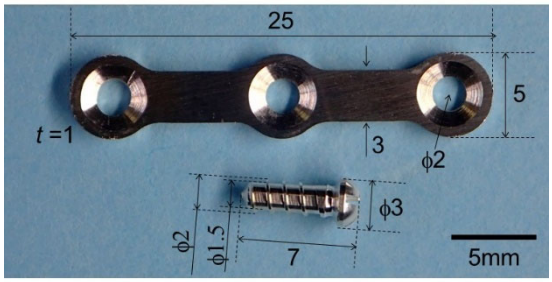


Figure 1. Appearance and dimensions of MgCa plate and screw.

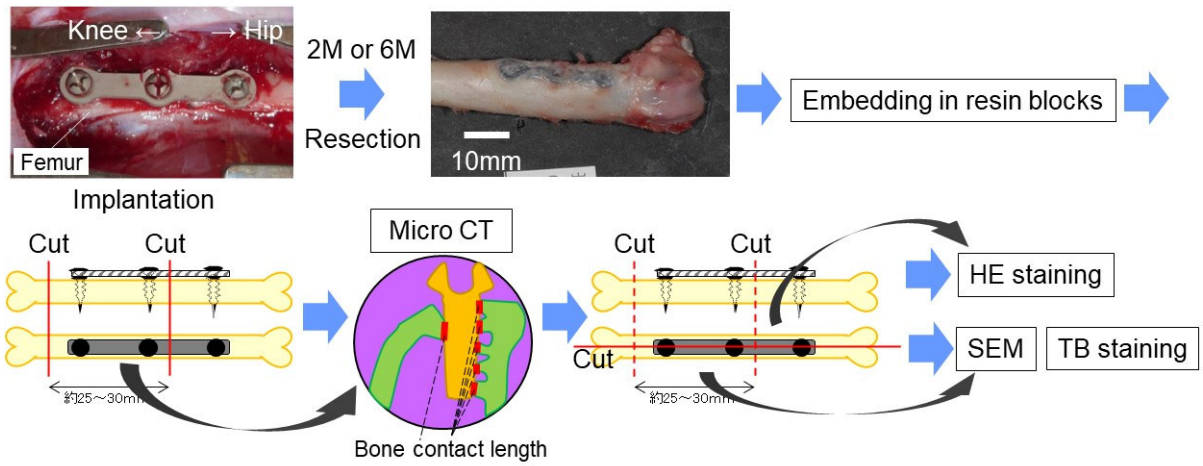


Figure 2. Experimental procedure.

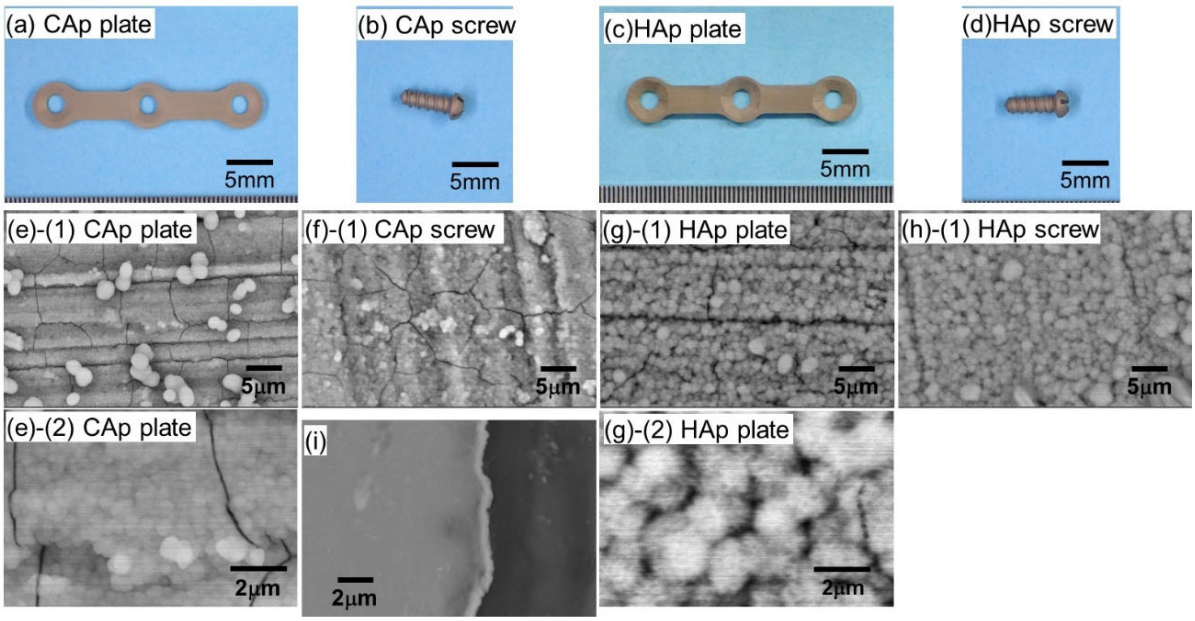


Figure 3. Optical images of (a) CAp-coated plate, (b) CAp-coated screw, (c) HAp-coated plate, and (d) HAp-coated screw. Surface SEM images of (e) CAp-coated plate, (f) CAp-coated screw, (g) HAp-coated plate, and (h) HAp-coated screw with (1) low and (2) high magnifications. (i) Cross-sectional SEM image of CAp-coated screw.

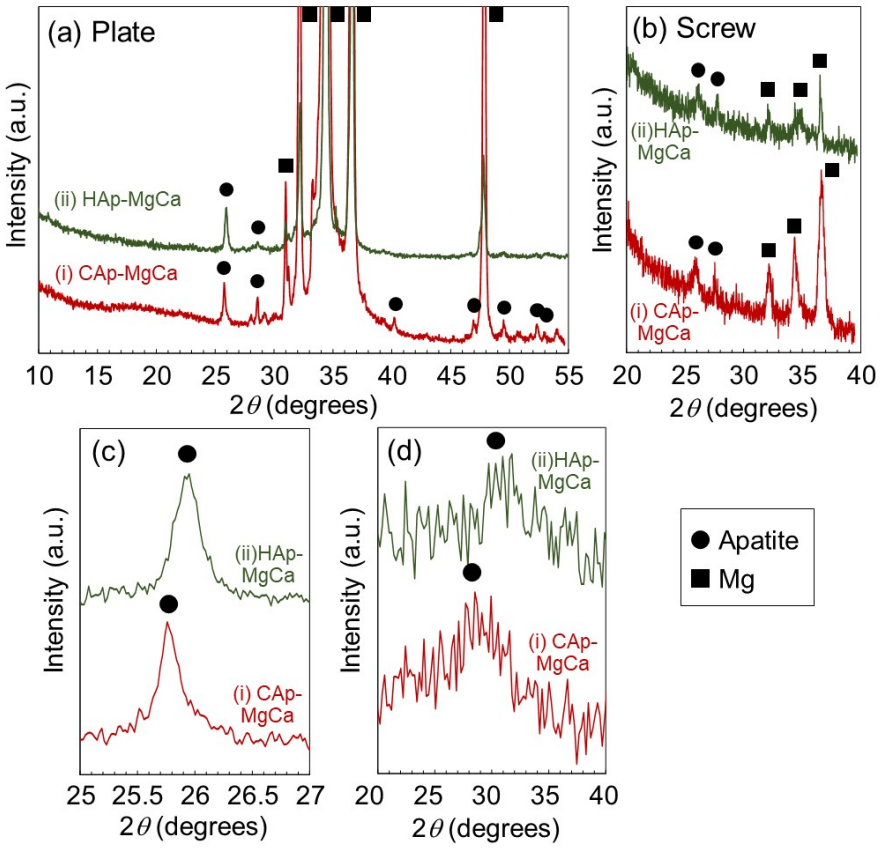


Figure 4. (a) and (b) Wide range XRD patterns and (c) and (d) magnified apatite 002 plane diffraction peak of (a) and (c) plate and (b) and (d) screw with (i) CAp and (ii) HAp coatings.

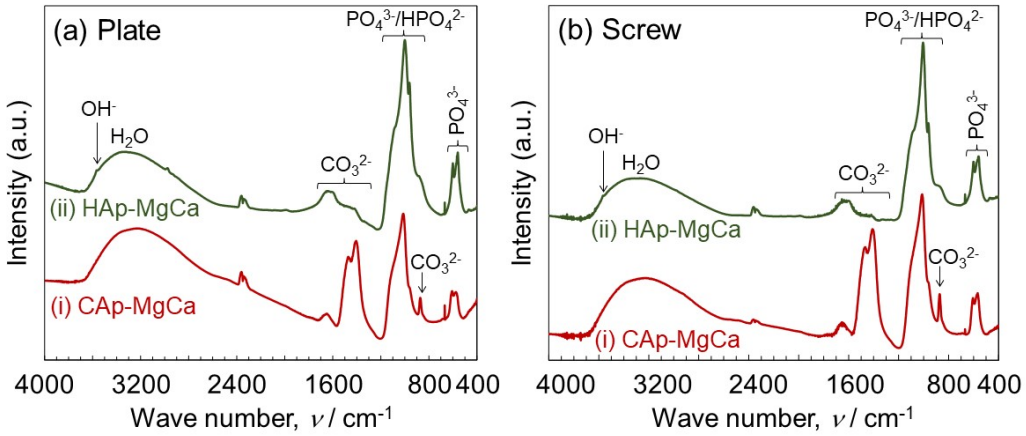


Figure 5. FTIR spectra of (a) plate and (b) screw with (i) CAp and (ii) HAp coatings.

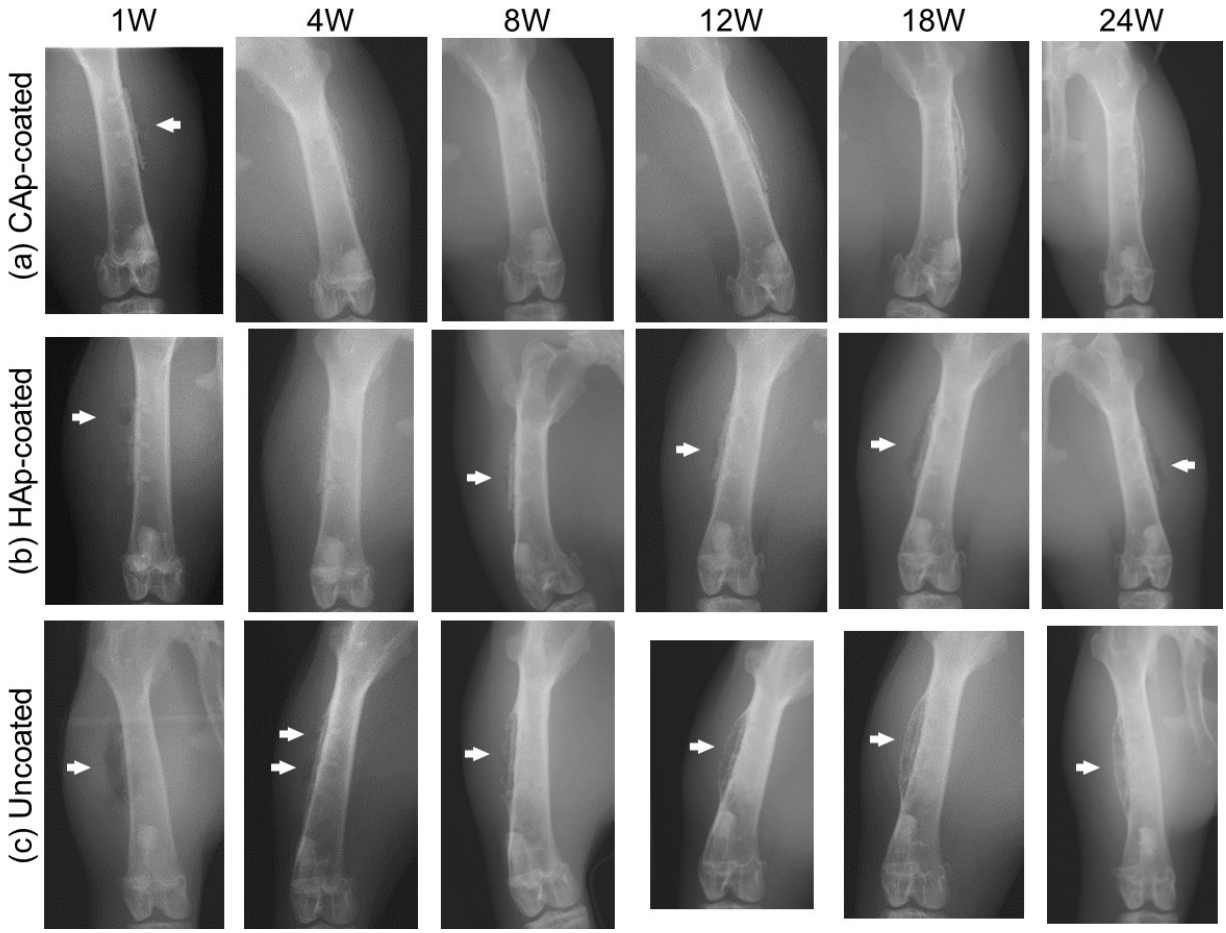


Figure 6. X-ray photographs of femurs with (a) CAp-coated, (b) HAp-coated and (c) uncoated devices implanted for 1, 4, 8, 12, 18 and 24 weeks.

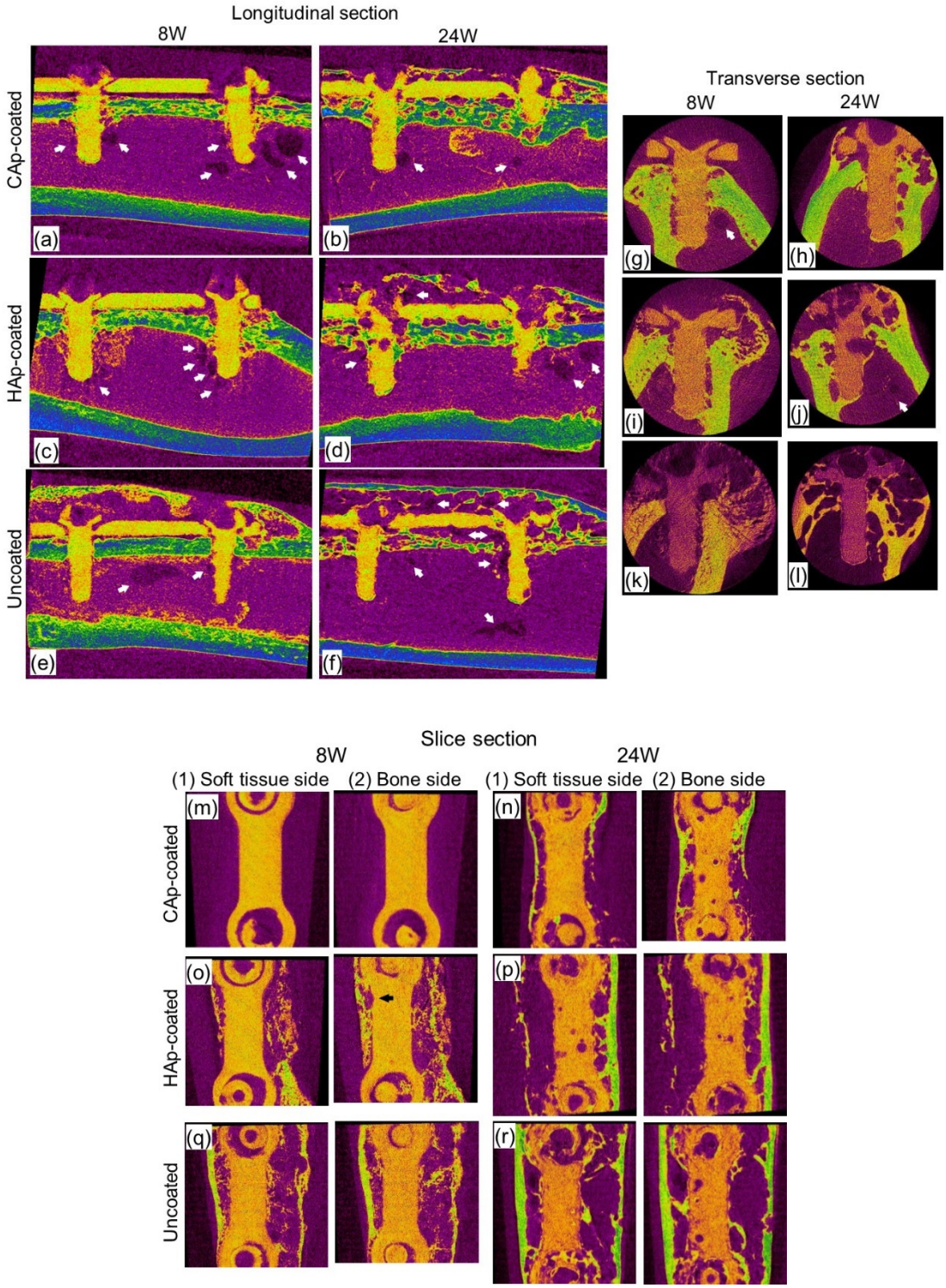


Figure 7. X-ray μCT images of (a)-(f) longitudinally sectioned femurs with plate and screw, (g)-(l) transversely sectioned femur with screw and (m)-(r) horizontally sliced plates, implanted for 8 and 24 weeks. (a), (b), (g), (h), (m) and (n) CAp-coated, (c), (d), (i), (j), (o) and (p) HAp-coated and (e), (f), (k), (l), (q) and (r) uncoated devices. Yellow substance: metal, blue substance: original bone, yellow and green substance: new bone, and dark area: gas cavity.

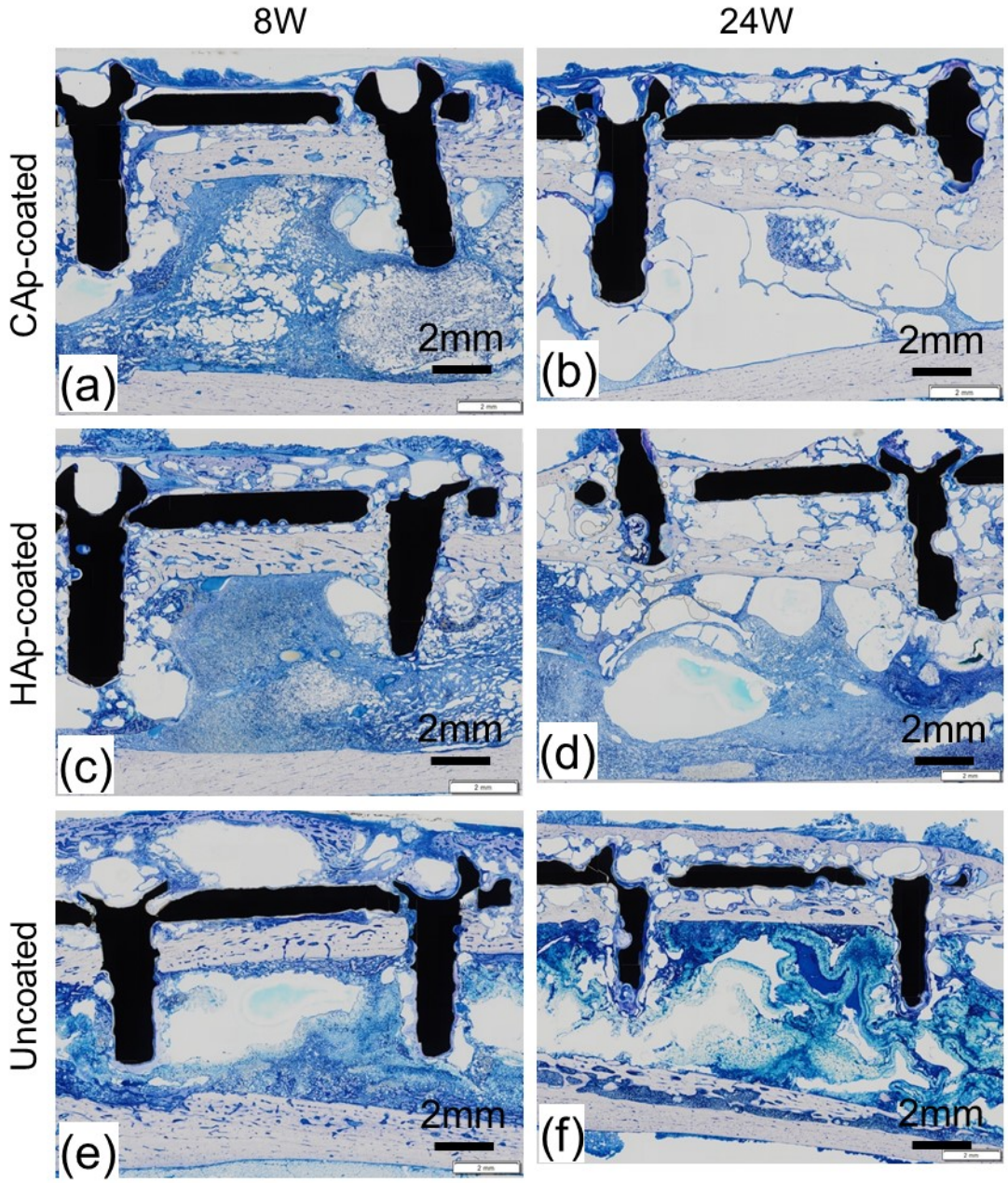


Figure 8. TB-stained longitudinal cross-sectional images of femurs with (a) and (b) CAp-coated, (c) and (d) HAp-coated and (e) and (f) uncoated MgCa devices implanted for (a), (c) and (e) 8 weeks and (b), (d) and (f) 24 weeks.

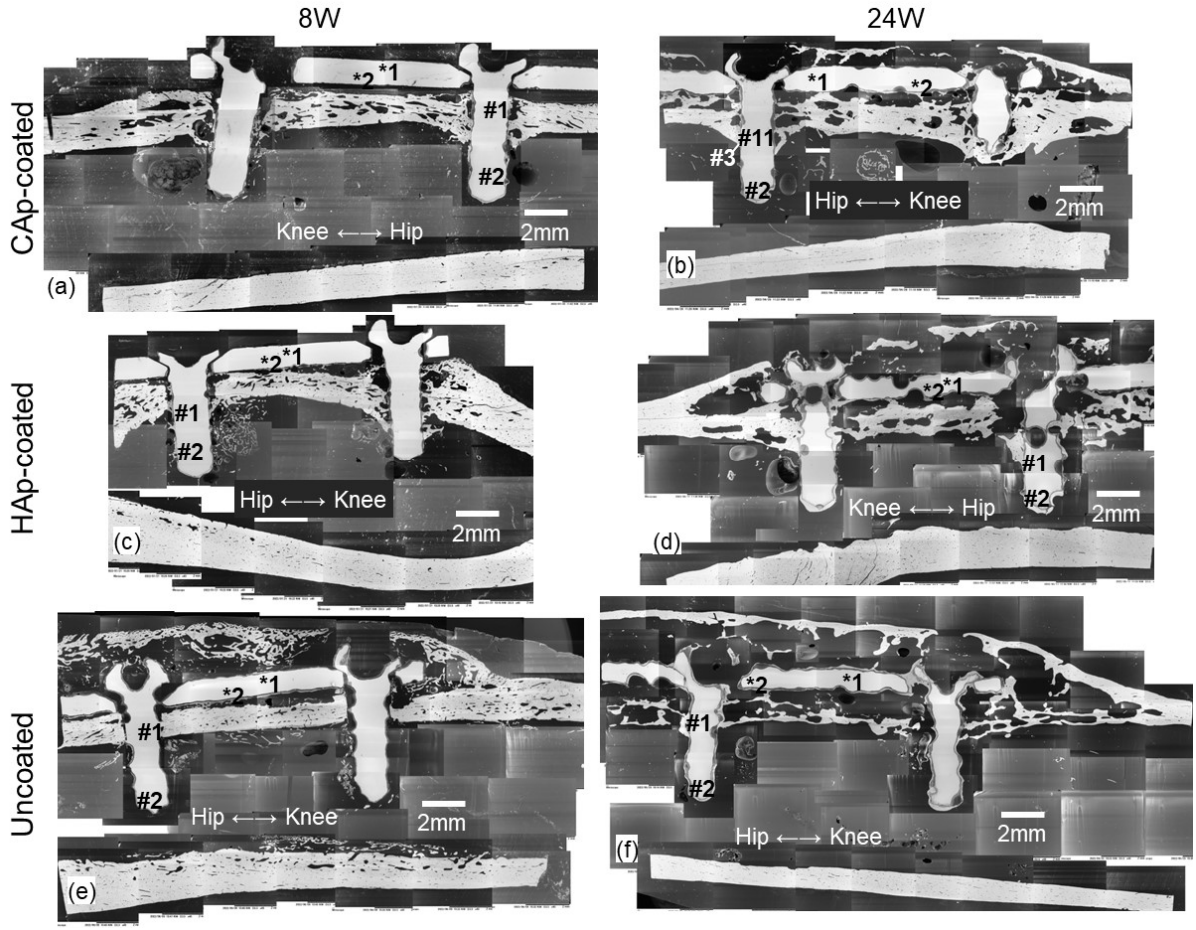


Figure 9. SEM images of longitudinal cross section of femurs with (a) and (b) CAp-coated, (c) and (d) HAp-coated and (e) and (f) uncoated MgCa devices implanted for (a), (c) and (e) 8 weeks and (b), (d) and (f) 24 weeks. Bright contrasting substance: metal, dark grey contrasting substance on metal: corrosion product consisting mainly of $Mg(OH)_2$, light grey contrasting substance: bone, bright contrasting dense substance on $Mg(OH)_2$ layer: calcium phosphate, and darkest contrasting substance: embedded resin, according to EDS analysis.

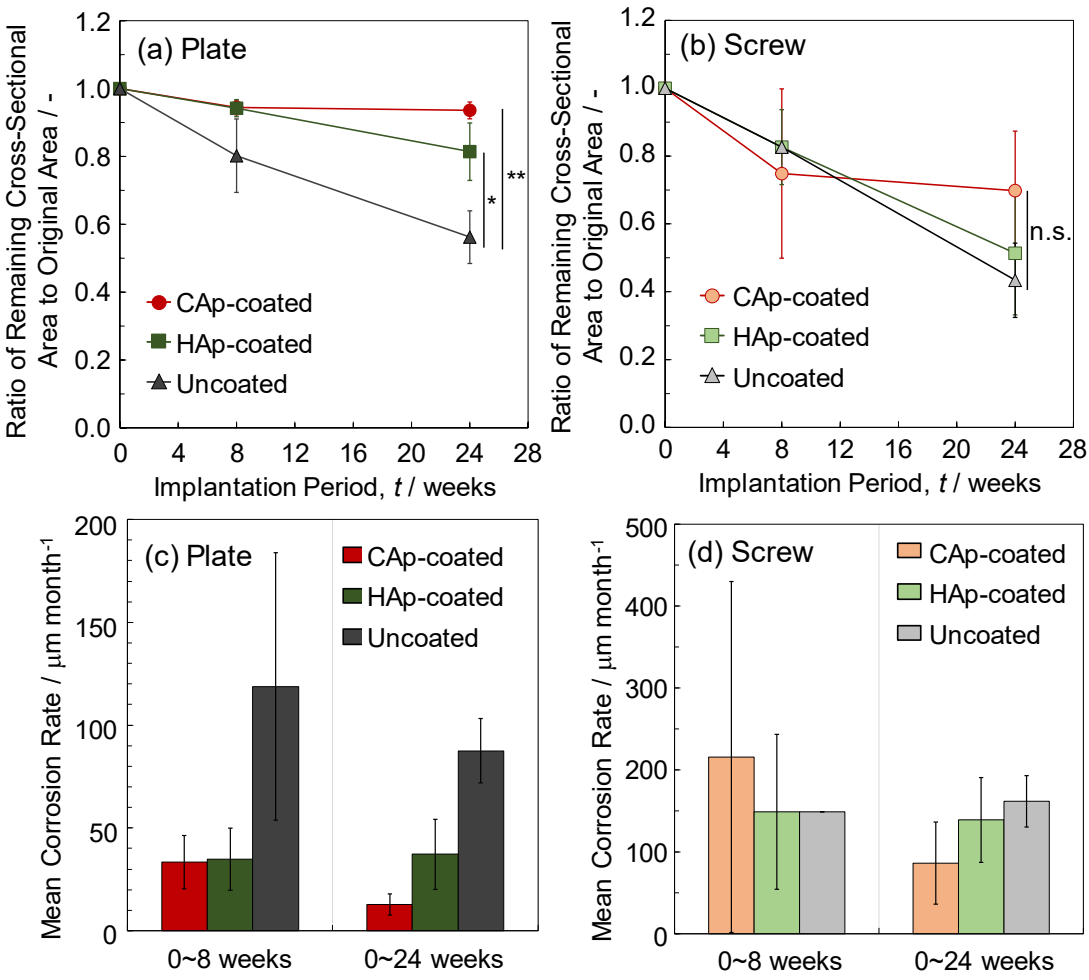


Figure 10. (a) and (b) Ratio of remaining cross-sectional area to the original area and (c) and (d) mean corrosion rate for 8 and 24 weeks of CAp-coated, HAp-coated and uncoated (a) and (c) plate and (b) and (d) screw. n.s.: not significant, *: $p<0.05$, **: $p<0.01$.

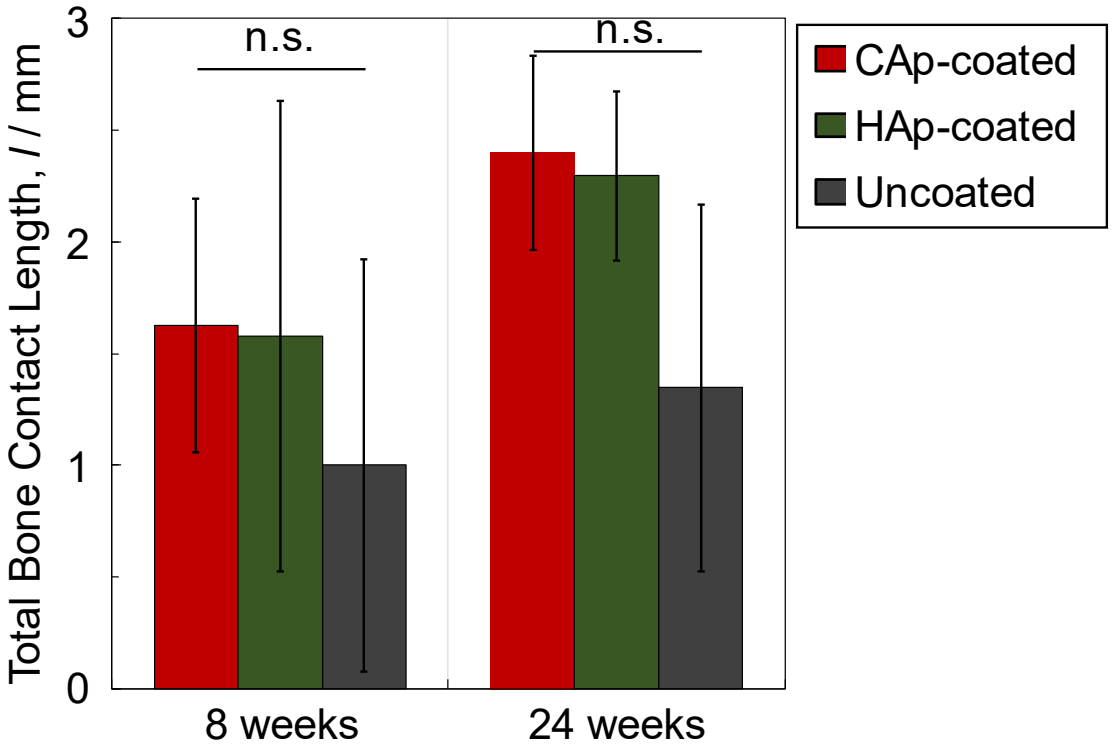


Figure 11. Total bone contact length of MgCa screws with and without CAp and HAp coatings implanted for 8 and 24 weeks. n.s.: not significant.

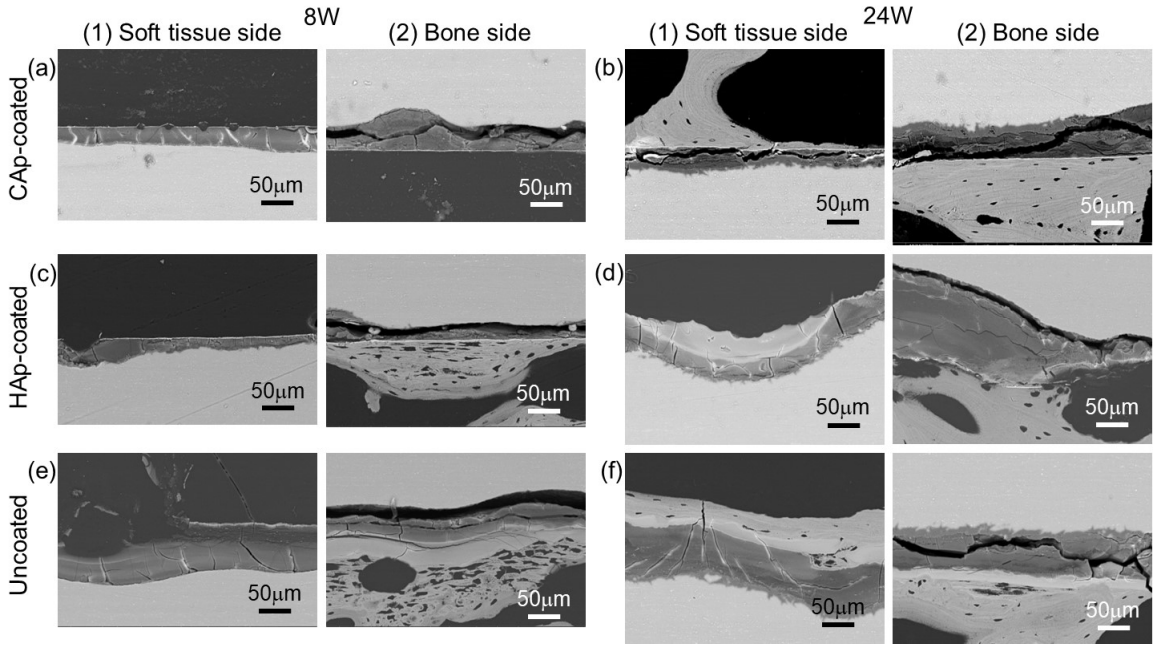


Figure 12. Magnified SEM images of near surface areas on (a) and (b) CAp-coated, (c) and (d) HAp-coated and (e) and (f) uncoated plates implanted for (a), (c) and (e) 8 weeks and (b), (d) and (f) 24 weeks. (1) soft-tissue side and (2) bone sides of plate marked with *1 and *2 in Fig. 9, respectively.

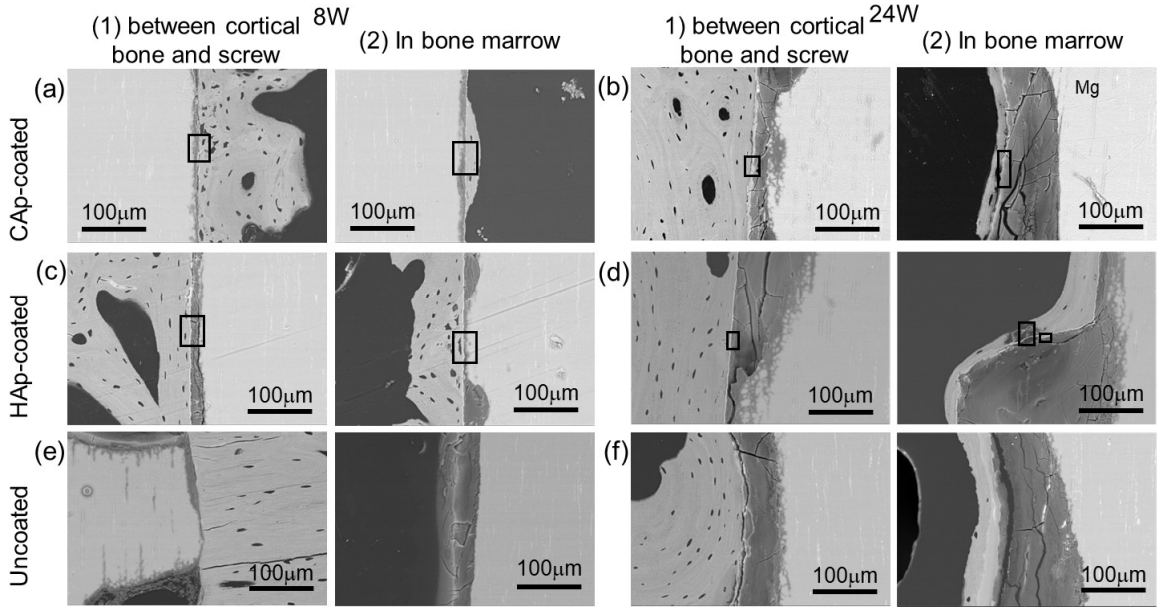


Figure 13. Magnified SEM images of near surface areas on (a) and (b) CAp-coated, (c) and (d) HAp-coated and (e) and (f) uncoated screws implanted for (a), (c) and (e) 8 weeks and (b), (d) and (f) 24 weeks. (1) area between cortical bone and screw and (2) area in bone marrow of screw marked with #1 and #2 in Fig. 9, respectively.

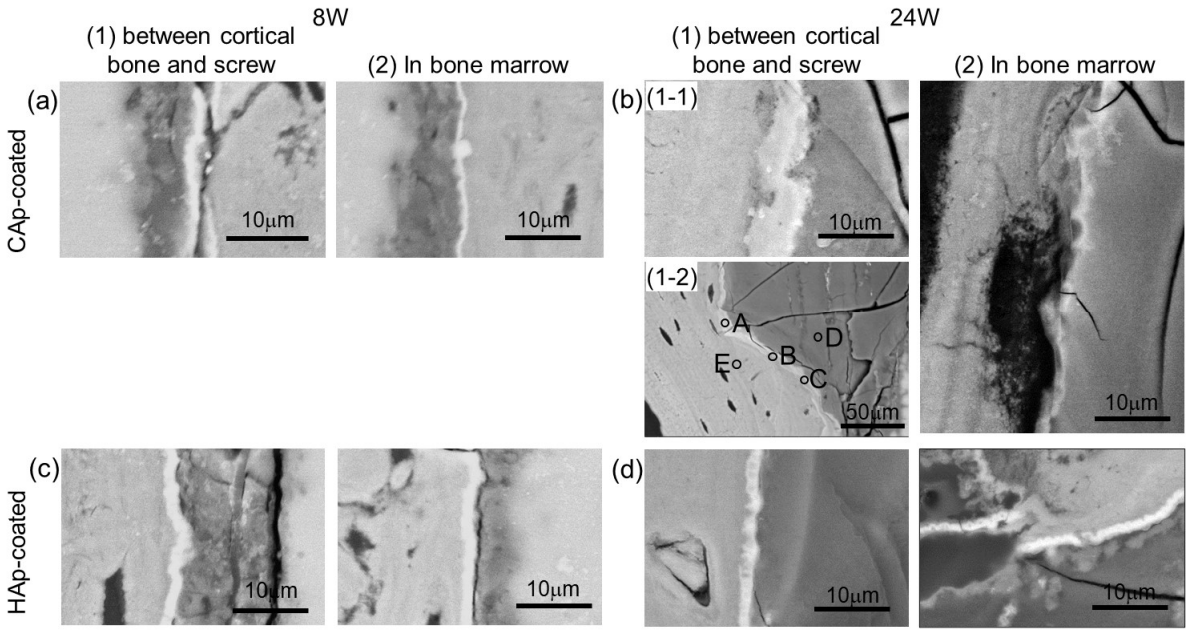


Figure 14. Highly magnified SEM images of (a) and (b) CAp coating and (c) and (d) HAp coating (1) at boundary between cortical bone and screw and (2) in bone marrow encircled on Fig. 12, implanted for (a) and (c) 8 weeks and (b) and (d) 24 weeks.

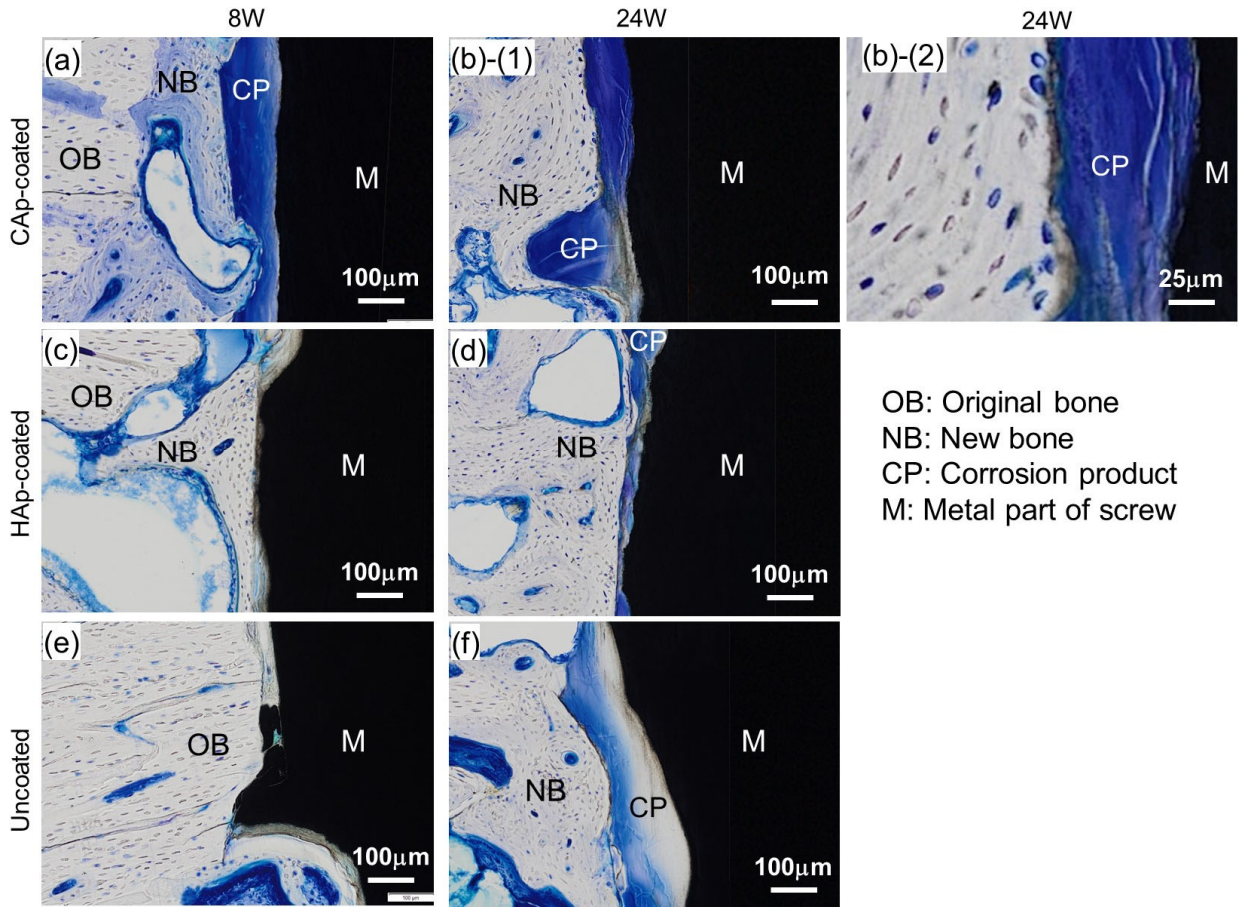


Figure 15. Magnified TB-stained images of boundary between cortical bone and (a) and (b) CAp-coated, (c) and (d) HAp-coated and (e) and (f) uncoated screws implanted for (a), (c) and (e) 8 weeks and (b), (d) and (f) 24 weeks.

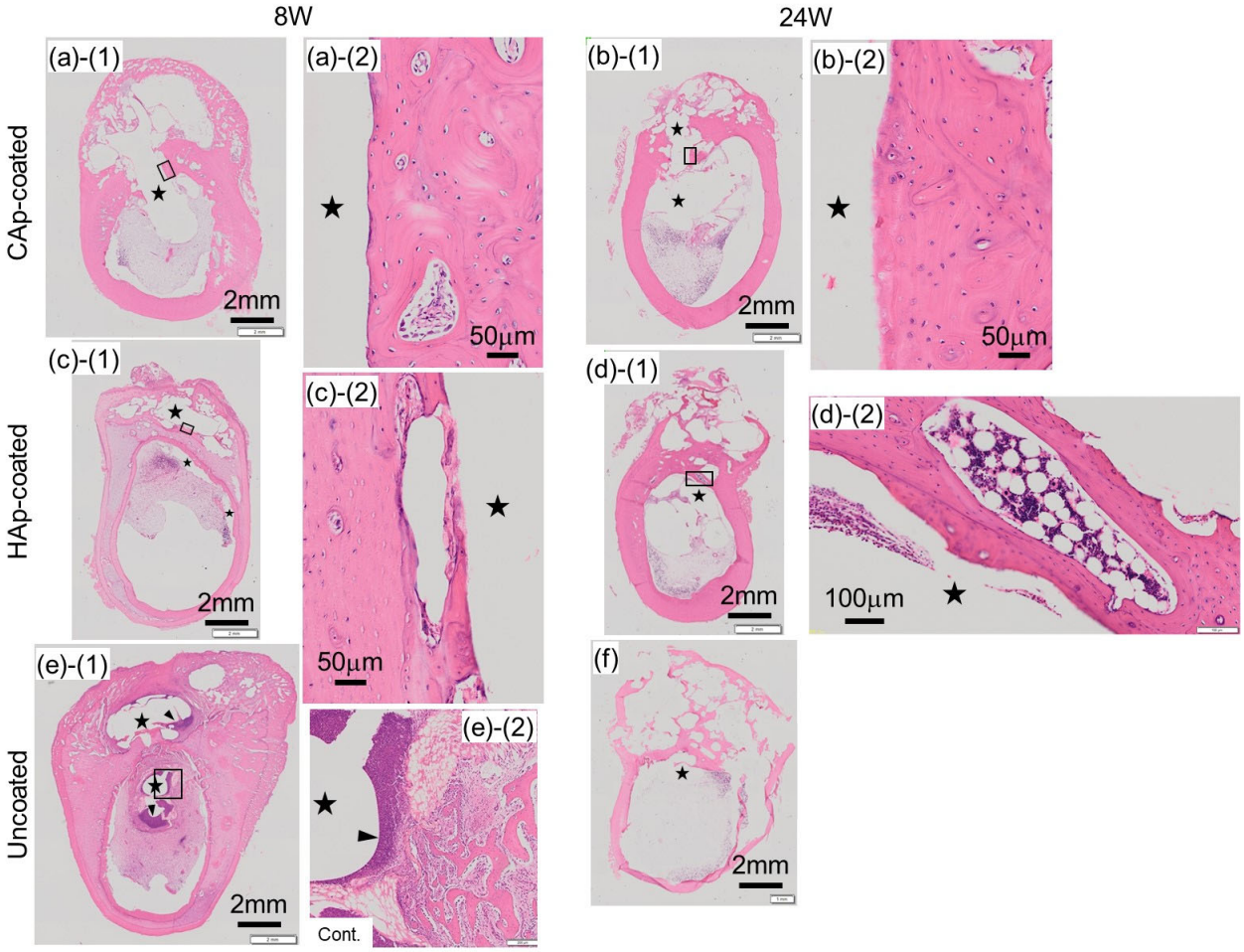


Figure 16. HE-stained transverse cross-sectional images of femurs with (a) and (b) CAp-coated, (c) and (d) HAp-coated and (e) and (f) uncoated screws implanted for (a), (c) and (e) 8 weeks and (b), (d) and (f) 24 weeks. (1) Low magnification image and (2) high magnification image of the squared area on image (1). Star mark indicates where screw and plate were located.